Theoretical study of the radiative capture reactions ^{2}H(n,γ) ^{3}H and ^{2}H(p,γ) ^{3}He at low energies

M. Viviani

Istituto Nazionale di Fisica Nucleare, Sezione di Pisa, I-56100 Pisa, Italy

R. Schiavilla

CEBAF Theory Group, Newport News, Virginia 23606
and Department of Physics, Old Dominion University, Norfolk, Virginia 23529

A. Kievsky

Istituto Nazionale di Fisica Nucleare, Sezione di Pisa, I-56100 Pisa, Italy

Correlated hyperspherical harmonics wave functions with Δ-isobar admixtures obtained from realistic interactions are used to study the thermal neutron radiative capture on deuterium, and the ^{2}H$(\vec{p},\gamma)$ ^{3}He and $p(\vec{d},\gamma)$ ^{3}He reactions in the center of mass energy range 0–100 keV. The nuclear electromagnetic current includes one- and two-body components. Results for the ^{2}H$(\vec{n},\gamma)$ ^{3}H cross section and photon polarization parameter, as well as for the energy dependence of the astrophysical factor and angular distributions of the differential cross section, vector and tensor analyzing powers, and photon linear polarization coefficient of the ^{2}H$(\vec{p},\gamma)$ ^{3}He and $p(\vec{d},\gamma)$ ^{3}He reactions are reported. Large effects due to two-body currents, in particular the long-range ones associated with the tensor component of the nucleon-nucleon interaction, are observed in the photon polarization parameter and vector analyzing power. Good, quantitative agreement between theory and experiment is found for all observables, with the exception of the vector analyzing power for which the calculated values underestimate the data by about 30%. [S0556-2813(96)03508-X]

PACS number(s): 21.45.+v, 24.70.+s, 25.40.Lw, 27.10.+h

I. INTRODUCTION

Very low-energy radiative and weak capture reactions involving few-nucleon systems have considerable astrophysical relevance for studies of stellar structure and evolution [1], and big-bang nucleosynthesis [2]. Three such aspects are (1) the mechanism for the energy and neutrino production in main sequence stars, in particular the determination of the solar neutrino flux; (2) the process of protostellar evolution towards the main sequence; (3) the predictions for the primordial abundances of light elements.

These same reactions are also very interesting from the standpoint of the theory of strongly interacting systems, since their cross sections are very sensitive to the model used to describe both the ground state and continuum wave functions, and the two-body electroweak current operators. Indeed, calculations of the ^{2}H(n,γ) ^{3}H and ^{3}He(n,γ) ^{4}He capture cross sections at thermal neutron energies carried out with realistic wave functions and a single-nucleon electromagnetic current, the so-called impulse approximation (IA), predict only about 50% [3] and 10% [4] of the corresponding experimental values. This is because the IA transition operator cannot connect the main S-state components of the deuteron and triton, or ^{3}He and ^{4}He, wave functions. Hence, the calculated cross section in the IA is small, since the reaction must proceed through the small components of the wave functions, in particular the mixed symmetry S'-state admixture. Two-body currents, however, do connect the dominant S-state components, and the associated matrix elements are exceptionally large in comparison to those obtained in IA.

The focus of the present study is on the ^{2}H(p,γ) ^{3}He

reaction with proton laboratory energies in the range 0–150 keV, and the thermal neutron radiative capture on deuterium. The cross section for the latter process was most recently measured to be $\sigma_T = 0.508 \pm 0.015$ mb [5], in agreement with the results of earlier experiments [6,7]. In the late 1980s, measurements of both the photon polarization following polarized neutron capture [8], and γ emission after polarized neutron capture from polarized deuterons [9] were also carried out.

In an experiment performed last year at TUNL [10,11], the total cross section and vector and tensor analyzing powers of the ^{2}H$(\vec{p},\gamma)$ ^{3}He and $p(\vec{d},\gamma)$ ^{3}He reactions were measured at center of mass energies below 55 keV. The astrophysical S factor, extrapolated to zero energy from the cross section data, was found to be $S(E_{\text{c.m.}}=0)=0.165\pm0.014$ eV b, where the error includes both systematic and statistical uncertainties [11]. This value for $S(0)$ is about 35% smaller than that obtained by Griffith *et al.* [12] more than 30 years ago, the only other experimental determination of $S(0)$ which we are aware of. More recently, in another experiment performed at TUNL, a different group [13] has extended the study of the ^{2}H$(\vec{p},\gamma)$ ^{3}He and $p(\vec{d},\gamma)$ ^{3}He reactions at center of mass energies between 75 and 300 KeV.

The theory of the ^{2}H(n,γ) ^{3}H capture reaction has a long history. The ''pseudo-orthogonality'' between the ^{3}H ground state and nd doublet or quartet state inhibiting the M_1 transition in the IA for this process, and thus explaining the smallness of its cross section when compared to that for the $p(n,\gamma)$ ^{2}H reaction, $\sigma_T = 334.5 \pm 0.5$ mb, was first pointed out by Schiff [14]. Later, Phillips [15] emphasized the importance of initial state interactions and two-body cur-

rents to the capture reaction in a three-body model calculation, by considering a central, separable interaction. In more recent years, a series of calculations of increasing sophistication with regard to the description of both the initial and final state wave functions and two-body current model were carried out [16,17]. These efforts culminated in the 1990 Friar *et al.* [3] calculation of the ^{2}H(n,γ)^{3}H total cross section, quartet capture fraction, and photon polarization, based on converged bound and continuum state Faddeev wave functions, corresponding to a variety of realistic Hamiltonian models with two- and three-nucleon interactions, and a nuclear electromagnetic current operator, including the long-range two-body components associated with pion exchange and the virtual excitation of intermediate Δ resonances. Within this framework, Friar *et al.* clearly showed the importance of initial state interactions and two-body current contributions. They also showed that both the calculated cross section and photon polarization parameter could be in good, quantitative agreement with the experimental values, if the cutoff Λ_π at the πNN vertices in the two-body currents was taken in the range 1050 MeV $\leq \Lambda_\pi \leq$ 1200 MeV, depending on the particular combination of two- and three-body interactions considered.

The theoretical description of the ^{2}H(p,γ)^{3}He reaction at low energies is complicated by the presence of the Coulomb interaction. Only relatively recently has the S-wave capture contribution to the zero-energy S factor of this reaction been calculated with numerically converged Faddeev wave functions [18], obtained from realistic Hamiltonians including the Coulomb interaction. The calculated value for $S_S(0)$ has been found to be 0.108 eV b, in excellent agreement with its most recent experimental determination, $S_S(0) = 0.109 \pm 0.010$ eV b [11].

The recent, precise measurements of the astrophysical factor, vector and tensor analyzing powers $A_y(\theta)$ and $T_{20}(\theta)$, respectively, and photon linear polarization $P_\gamma(\theta)$ in the reactions ^{2}H$(\vec{p},\gamma)$^{3}He and $p(\vec{d},\gamma)$^{3}He [11,13] are the main motivation for the present work. The observed linear dependence upon the energy of the S factor as well as the observed angular distributions of the cross section and polarization observables indicate that these reactions proceed predominantly through S- and P-wave capture [11,13]. Such

S- and P-wave capture processes have not been previously theoretically studied at very low energies.

In the present work, the bound trinucleon and continuum Nd wave functions are obtained from realistic two- and three-nucleon interactions with a variational method consisting in their expansion over a pair-correlated-hyperspherical-harmonics (PHH) function basis [19–21]. The method has been shown to be very accurate, in the sense that results obtained for a variety of bound state and low-energy scattering observables are very close (typically, within less than 1%) in comparison to those obtained with converged Faddeev wave functions [22]. We also include one- and two-Δ-isobar components in the wave functions. These are generated with the transition-correlation-operator (TCO) method, developed in Ref. [23]. Both the PHH expansion and TCO method are reviewed in Sec. II. The model for the nuclear electromagnetic current, given in Sec. III, consists of one- and two-body terms. Since explicit expressions for the latter are scattered in a number of Refs. [4,24,25], we list them in Appendix A for completeness. Definitions for the cross section and polarization observables along with their expansion in electric and magnetic multipoles are given in Sec. IV and Appendix B, while the Monte Carlo calculation of the required matrix elements is discussed in Sec. V. Results for the ^{2}H$(\vec{n},\gamma)$^{3}H reaction at thermal neutron energy, and the ^{2}H$(\vec{p},\gamma)$^{3}He and ^{1}H$(\vec{d},\gamma)$^{3}He reactions with center of mass energies in the range 0–100 keV are presented, and compared with data in Sec. VI. Finally, Sec. VII contains a concluding discussion.

II. BOUND- AND SCATTERING-STATE WAVE FUNCTIONS

A. Bound-state wave functions

In a series of recent papers, a variational technique for calculating the trinucleon bound-state and Nd scattering-state wave functions has been developed [19–21]. The method consists of the expansion of the three-body wave functions on a basis of pair-correlated hyperspherical harmonic (PHH) functions, and is briefly reviewed here. For the trinucleon bound state, the wave function is written as

$$\Psi_3^{JJ_z} = \sum_{\alpha=1}^{N_c} \sum_{K=K_m^\alpha}^{K_M^\alpha} \frac{u_{\alpha K}(\rho)}{\rho^{5/2}} \sum_{ijk \text{ cyclic}} f_\alpha(r_{jk})^{(2)}P_K^{\ell_\alpha,L_\alpha}(\phi_i) \mathcal{Y}_\alpha^{JJ_z}(jk,i), \qquad (2.1)$$

$$\rho = \sqrt{x_i^2 + y_i^2}, \qquad (2.2)$$

$$\cos\phi_i = x_i/\rho, \qquad (2.3)$$

where $\mathbf{x}_i = \mathbf{r}_j - \mathbf{r}_k$ and $\mathbf{y}_i = (\mathbf{r}_j + \mathbf{r}_k - 2\mathbf{r}_i)/\sqrt{3}$, $\mathbf{r}_i$ denoting the position of particle i. The angle-spin-isospin functions $\mathcal{Y}_\alpha(jk,i)$ are defined as

$$\mathcal{Y}_\alpha^{JJ_z}(jk,i) = \{[Y_{l_\alpha}(\hat{\mathbf{x}}_i) \otimes Y_{L_\alpha}(\hat{\mathbf{y}}_i)]_{\Lambda_\alpha}[s_\alpha^{jk} \otimes s_\alpha^i]_{S_\alpha}\}_{JJ_z}[t_\alpha^{jk} \otimes t_\alpha^i]_{TT_z}. \qquad (2.4)$$

Each α channel is specified by the orbital angular momenta ℓ_α and L_α coupled to give Λ_α, and by the spin (isospin) s_α^{jk} (t_α^{jk}) and s_α^i (t_α^i) of the pair jk and the third particle i, coupled to give S_α (T). Since the wave function Ψ_3 is antisymmetric, $\ell_\alpha + s_\alpha^{jk} + t_\alpha^{jk}$ must be odd; furthermore, $\ell_\alpha + L_\alpha$ must be even or odd depending on whether the state has even or odd parity. The hyperspherical polynomials $^{(2)}P_K^{\ell_\alpha,L_\alpha}$ are given by [26]

$$^{(2)}P_K^{\ell_\alpha,L_\alpha}(\phi_i) = N_n^{\ell_\alpha,L_\alpha}(\sin\phi_i)^{L_\alpha}(\cos\phi_i)^{\ell_\alpha}P_n^{L_\alpha+1/2,\ell_\alpha+1/2}(\cos 2\phi_i), \tag{2.5}$$

where $N_n^{\ell_\alpha,L_\alpha}$ is a normalization factor, and $P_n^{(a,b)}$ are Jacobi polynomials. The grand orbital quantum number is given by $K = \ell_\alpha + L_\alpha + 2n$, n being a non-negative integer. In Eq. (2.1), $K_m^\alpha = \ell_\alpha + L_\alpha$ is the minimum grand orbital quantum number and K_M^α is its maximum selected value, so that the number of basis functions per channel is

$$M_\alpha = (K_M^\alpha - K_m^\alpha)/2 + 1. \tag{2.6}$$

The pair-correlation functions $f_\alpha(r_{ij})$ take into account the strong state-dependent correlations induced by the nucleon-nucleon interaction, and are obtained as the solutions of suitable two-body zero-energy Schrödinger equations, with a technique outlined in Ref. [19]. They improve the behavior of the wave function at small interparticle distances, thus accelerating the convergence of the calculated quantities with respect to the required number of basis functions in Eq. (2.1). With the f_α set equal to one, as in the original hyperspherical-harmonic expansion approach [27], the convergence rate slows down considerably, making the calculations very difficult for systems, such as nuclei, having strongly repulsive interactions at short distances.

The Rayleigh-Ritz variational principle

$$\langle \delta_u\Psi_3 | H - E | \Psi_3 \rangle = 0, \tag{2.7}$$

is used to determine the hyperradial functions $u_{\alpha K}(\rho)$ in Eq. (2.1). Here $\delta_u\Psi_3$ represents the change in the wave function due to variations of the functions $u_{\alpha K}(\rho)$. For a given N_c and K_M^α the resulting set of coupled second-order differential equations is solved by using standard numerical methods. Typically, $N_c = 10$–18 and $M_\alpha = 5$–8. Finally, we note that inclusion of the Coulomb interaction is straightforward in the present approach, since no partial wave decomposition is performed.

B. Scattering-state wave functions

The variational approach based on the PHH function basis has been extended to study scattering states. The wave function for an Nd scattering state is written as

$$\Psi_{2+1}^{LSJJ_z} = \Psi_C^{LSJJ_z} + \Psi_A^{LSJJ_z}, \tag{2.8}$$

where J and J_z are, respectively, the total angular momentum and its z projection, L is the Nd relative orbital angular momentum, and S the channel spin quantum number. The first term Ψ_C must guarantee an accurate description of the system in the region where the N and d clusters are close to each other, and interparticle interactions are large; it vanishes in the limit of large Nd distances. As for the bound-state problem, Ψ_C is expanded in terms of PHH functions.

The second term Ψ_A in Eq. (2.8) describes the asymptotic configurations of the system, where the nuclear interactions between the two clusters are negligible. For a pd state, it is written as [20]

$$\Psi_A^{LSJJ_z} = \frac{1}{\sqrt{3}} \sum_{ijk\,\text{cyclic}} \sum_{L'S'} \{[s^i \otimes \phi_d(\mathbf{x}_i)]_{S'} \otimes Y_{L'}(\hat{\mathbf{y}}_i)\}_{JJ_z}[t^i \otimes [t^j \otimes t^k]_0]_{(1/2)T_z}$$

$$\times \left[\delta_{LL'}\delta_{SS'}\frac{F_{L'}(pr_{pd})}{pr_{pd}} + {}^J R_{LS}^{L'S'}\frac{G_{L'}(pr_{pd})}{pr_{pd}}g(r_{pd}) \right], \tag{2.9}$$

where ϕ_d is the radial-spin part of the deuteron wave function, p the magnitude of the relative momentum $\mathbf{p}$ between deuteron and proton, and F_L and G_L are the regular and irregular Coulomb functions, respectively. For nd scattering, $F_L(x)/x$ [$G_L(x)/x$] is replaced by the regular (irregular) spherical Bessel function. The function $g(r_{pd})$ modifies the $G_L(pr_{pd})$ at small r_{pd} by regularizing it at the origin, and approaches one for $r_{pd} > 10$ fm, thus not affecting the asymptotic behavior of $\Psi_{2+1}^{LSJJ_z}$. The sum over $L'S'$ is over all values compatible with a given J and parity.

The R-matrix elements ${}^J R_{LS}^{L'S'}$ and the functions $u_{\alpha K}(\rho)$ in the PHH expansion of Ψ_C are determined variationally by finding the stationary points of the functional [20]

$$[{}^J R_{LS}^{L'S'}] = {}^J R_{LS}^{L'S'} - \left\langle \psi_{2+1}^{LSJJ_z} \left| H - E_d - \frac{p^2}{2\mu} \right| \psi_{2+1}^{LSJJ_z} \right\rangle, \tag{2.10}$$

with respect to variations in the ${}^J R_{LS}^{L'S'}$ and $u_{\alpha K}$ (Kohn variational principle). Here $E_d = -2.225$ MeV is the deuteron ground-state energy, and μ the Nd reduced mass. As in the

TABLE I. Binding energies and scattering lengths corresponding to the AV14, AV14/VIII, and AV18/IX Hamiltonian models. The AV14 results obtained with the PHH expansion are compared with those calculated by solving the Faddeev equations in configuration (Faddeev/R) and in momentum (Faddeev/Q) space. The measured scattering lengths are from [35].

Hamiltonian	Method	^{3}H B (MeV)	nd ^2a (fm)	nd ^4a (fm)	^{3}He B (MeV)	pd ^2a (fm)	pd ^4a (fm)
	PHH	7.683	1.196	6.380	7.032	0.954	13.779
AV14	Faddeev/Q	7.680 [a]	1.200 [b]	6.388 [b]			
	Faddeev/R	7.670 [c]	1.200 [d]	6.372 [d]	7.014 [c]	0.965 [d]	13.764 [d]
AV14/VIII	PHH	8.48	0.59	6.37	7.80	−0.14	13.8
AV18/IX	PHH	8.49	0.63	6.33	7.75	−0.02	13.7
	expt.	8.48	0.65(2)	6.33(3)	7.72		

[a]Reference [32].
[b]Reference [22].
[c]Reference [33].
[d]Reference [34].

bound-state problem, the hyperradial functions $u_{\alpha K}(\rho)$ are required to vanish in the limit of large ρ.

C. Ground-state energies and Nd scattering lengths

The calculations carried out in the present study are for the following combinations of realistic two- and three-nucleon interactions: (1) the Argonne v_{14} two-nucleon interaction (AV14) [28]; (2) the Argonne v_{14} two-nucleon and Urbana model-VIII three-nucleon [29] interactions (AV14/VIII); (3) the Argonne v_{18} two-nucleon [30] and Urbana model-IX three-nucleon [31] interactions (AV18/IX). The v_{18} model contains explicit charge-independence and charge-symmetry breaking terms, as well as a complete treatment of the NN electromagnetic interaction, including magnetic moment, two-photon-exchange, Darwin-Foldy, and vacuum polarization corrections to the Coulomb interaction. It also has a weaker tensor component than the older Argonne v_{14} model.

The calculated ^{3}H and ^{3}He binding energies, and nd and pd doublet and quartet scattering lengths are reported in Table I, along with the (available) experimental values. We note that the strength of the three-nucleon interaction is, in each case, adjusted to reproduce the triton and α-particle experimental binding energies in converged Faddeev [29,36] and Green's function Monte Carlo [31,37] calculations. As the value of the doublet nd scattering length is correlated with that of the triton binding energy [38], both the AV14/VIII and AV18/IX Hamiltonian models predict very well the measured ^2a. Without the three-nucleon interaction, the ^2a value is overestimated by almost a factor of 2. In contrast, the quartet scattering length ^4a has very little dependence on the Hamiltonian model, since in that channel the process is dominated by repulsive Pauli principle effects.

D. Nuclear wave functions with explicit Δ-isobar components

Following a method originally proposed in Ref. [23], explicit Δ-isobar components are approximately included in the nuclear wave functions by writing

$$\Psi = \left[S \prod_{i<j} (1 + U_{ij}^{TR}) \right] \Psi_N, \qquad (2.11)$$

where S is the symmetrizer, Ψ_N contains only nucleon degrees of freedom, and the transition operators U_{ij}^{TR} are defined as

$$U_{ij}^{TR} = U_{ij}^{N\Delta} + U_{ij}^{\Delta N} + U_{ij}^{\Delta\Delta}, \qquad (2.12)$$

$$U_{ij}^{N\Delta} = [u^{\sigma\tau II}(r_{ij})\sigma_i \cdot \mathbf{S}_j + u^{t\tau II}(r_{ij})S_{ij}^{II}]\tau_i \cdot \mathbf{T}_j, \qquad (2.13)$$

$$U_{ij}^{\Delta\Delta} = [u^{\sigma\tau III}(r_{ij})\mathbf{S}_i \cdot \mathbf{S}_j + u^{t\tau III}(r_{ij})S_{ij}^{III}]\mathbf{T}_i \cdot \mathbf{T}_j. \qquad (2.14)$$

Here, $\mathbf{S}_i$ and $\mathbf{T}_i$ are transition spin and isospin operators, which convert nucleon i into a Δ isobar; S_{ij}^{II} and S_{ij}^{III} are tensor operators in which the Pauli spin operators of particle i (or j), and particles i and j are replaced by corresponding spin-transition operators. The U_{ij}^{TR} vanishes in the limit of large interparticle separation, since no Δ components can exist asymptotically.

In principle, the U_{ij}^{TR} and Ψ_N could be determined variationally by using a Hamiltonian such as the Argonne v_{28Q} model [23,28], that contains both nucleon and Δ-isobar degrees of freedom. Instead we use transition correlations $u^{\sigma\tau II}(r_{ij})$, etc. (shown in Fig. 1) that approximately reproduce two-body bound-state and low-energy scattering wave functions for the Argonne v_{28Q} model, and take the PHH wave functions given above as the Ψ_N in Eq. (2.11). The validity of such an approximation has been discussed at length in Ref. [23]. Here we only note that (1) since the correlation functions $u^{\sigma\tau II}$, etc., are short-ranged, they are expected to be weakly A dependent; (2) it is important that the Ψ_N used in Eq. (2.11), obtained from the v_{14} interaction (phase equivalent to the v_{28Q} interaction), be proportional to that projected out from the full wave function for the v_{28Q} interaction. This has been explicitly verified by direct calculation in the two-body problem [23]. Finally, we note that the new Argonne v_{18} (nucleons only) interaction has no avail-
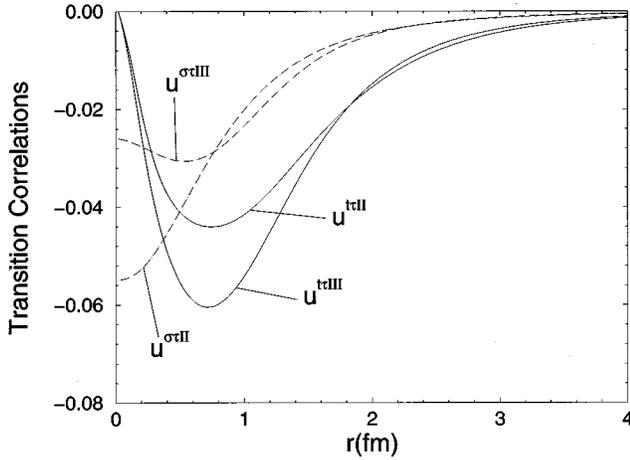
FIG. 1. Transition correlation functions obtained for the Argonne v_{28Q} interaction model.

able phase-equivalent nucleon and delta counterparts. Thus we insist on using the U_{ij}^{TR} obtained from the v_{28Q} model even when using in Eq. (2.11) the Ψ_N from the v_{18}. It is expected that this inconsistency has no significant impact on the results reported in the present work.

Δ-isobar components in nuclear wave functions are commonly estimated using first-order perturbation theory, and neglecting the kinetic energies in the denominators. Such calculations are equivalent to using Eq. (2.11) for the nuclear wave function with the components of U_{ij}^{TR} given by

$$U_{ij}^{N\Delta,PT} = \frac{v_{NN\to N\Delta}}{m-m_\Delta}, \qquad (2.15)$$

$$U_{ij}^{\Delta\Delta,PT} = \frac{v_{NN\to\Delta\Delta}}{2(m-m_\Delta)}, \qquad (2.16)$$

where $v_{NN\to N\Delta}$ and $v_{NN\to\Delta\Delta}$ are transition interactions (taken, in the present work, from the Argonne v_{28Q} model). This perturbative treatment has been shown to be inaccurate, and may lead to a substantial overprediction of the importance of Δ degrees of freedom in nuclei. For example, the cross section for the $^3\mathrm{He}(n,\gamma)^4\mathrm{He}$ reaction has been calculated to be, respectively, 112 μb and 86 μb [23] depending on whether Δ admixtures in the nuclear wave functions are included perturbatively or nonperturbatively, as outlined above.

III. THE NUCLEAR ELECTROMAGNETIC CURRENT

The nuclear electromagnetic current is expanded into a sum of one- and two-body terms that operate on the nucleon and Δ-isobar degrees of freedom [23]:

$$\mathbf{j}(\mathbf{q}) = \sum_i \mathbf{j}_i^{(1)}(\mathbf{q}) + \sum_{i<j} \mathbf{j}_{ij}^{(2)}(\mathbf{q}), \qquad (3.1)$$

where $\mathbf{q}$ is the photon momentum. The one-body term is written as

$$\mathbf{j}_i^{(1)}(\mathbf{q}) = \sum_{B,B'=N,\Delta} \mathbf{j}_i^{(1)}(\mathbf{q};B\to B'), \qquad (3.2)$$

with

$$\mathbf{j}_i^{(1)}(\mathbf{q};N\to N) = \frac{1}{4m}\{\mathbf{p}_i, e^{i\mathbf{q}\cdot\mathbf{r}_i}\}(1+\tau_{z,i}) - \frac{i}{4m}e^{i\mathbf{q}\cdot\mathbf{r}_i}\mathbf{q}$$
$$\times \sigma_i(\mu^s + \mu^v\tau_{z,i}), \qquad (3.3)$$

$$\mathbf{j}_i^{(1)}(\mathbf{q};N\to\Delta) = -\frac{i}{2m}\mu_{\gamma N\Delta}e^{i\mathbf{q}\cdot\mathbf{r}_i}\mathbf{q}\times\mathbf{S}_i T_{z,i}, \qquad (3.4)$$

$$\mathbf{j}_i^{(1)}(\mathbf{q};\Delta\to\Delta) = -\frac{i}{24m}\mu_{\gamma\Delta\Delta}e^{i\mathbf{q}\cdot\mathbf{r}_i}\mathbf{q}\times\Sigma_i(1+\Theta_{z,i}), \qquad (3.5)$$

where Σ (Θ) is the Pauli operator for the Δ spin (isospin), and the expression for $\mathbf{j}_i^{(1)}(\mathbf{q};\Delta\to N)$ is obtained from that for $\mathbf{j}_i^{(1)}(\mathbf{q};N\to\Delta)$ by replacing the transition spin and isospin operators by their Hermitian conjugates. Here $\mu^s=0.88\mu_N$ and $\mu^v=4.706\mu_N$ are the isoscalar and isovector nucleon magnetic moments in terms of nuclear magnetons μ_N; $\mu_{\gamma N\Delta}$ is taken equal to $3\mu_N$, as obtained from an analysis of γN data in the Δ resonance region [39]; $\mu_{\gamma\Delta\Delta}=4.35\mu_N$ by averaging the values recently obtained from a soft-photon analysis of pion-proton bremsstrahlung data near the Δ^{++} resonance [40]. Excitation of the Δ isobar via an electric quadrupole transition is neglected in the current $\mathbf{j}_i^{(1)}(\mathbf{q};N\to\Delta)$, since the associated pion photoproduction amplitude is experimentally found to be small at resonance [41]. We also note that in Eq. (3.5) the Δ-convection current is neglected.

Only $NN\to NN$ two-body terms are included in $\mathbf{j}_{ij}^{(2)}(\mathbf{q})$. These are separated into "model-independent" (MI) contributions, determined from the NN interaction (the Argonne v_{14} or v_{18} models in the present study) following a prescription originally proposed by Riska [42], and "model-dependent" (MD) ones associated with the $\rho\pi\gamma$ and $\omega\pi\gamma$ electromagnetic couplings:

$$\mathbf{j}_{ij}^{(2)} = \mathbf{j}_{ij,\mathrm{MI}}^{(2)} + \mathbf{j}_{ij,\mathrm{MD}}^{(2)}. \qquad (3.6)$$

Since the expressions for these MI and MD currents are scattered in a number of references [4,24,25], they are listed in Appendix A of this work for completeness. In principle, there are also two-body currents associated with the $NN\leftrightarrow N\Delta$ and $NN\leftrightarrow\Delta\Delta$ transitions. However, these have not been included in the present study.

The MD currents are purely transverse, and depend on a set of cutoff parameters and coupling constants only approximately known. Their contribution for momentum transfers $\leqslant 1$ GeV/c is small when compared to that of the MI currents [24]. The latter are constructed from the NN interaction so as to satisfy current conservation,

$$\mathbf{q}\cdot\mathbf{j}_{ij}^{(2)} = \left[v_{ij}, e^{i\mathbf{q}\cdot\mathbf{r}_i}\frac{1+\tau_{z,i}}{2} + i\to j\right], \qquad (3.7)$$

exactly [24,42]. While such a prescription cannot obviously be unique, it does lead to two-body currents, which have been shown to provide, at low and moderate values of momentum transfers (typically, below 1 GeV/c), a satisfactory description of the deuteron threshold electrodisintegration [25], ^{1}H$(n,\gamma)^2$H capture cross section at thermal neutron energies [25], and magnetic moments and form factors of the trinucleons [24,29].

The most important of the MI currents are those associated with the $v^{c\tau}(r_{ij})\tau_i\cdot\tau_j$, $v^{\sigma\tau}(r_{ij})\sigma_i\cdot\sigma_j\tau_i\cdot\tau_j$, and $v^{t\tau}(r_{ij})S_{ij}\tau_i\cdot\tau_j$ components of the interaction. The corresponding current operators are given in momentum space by [24]

$$\mathbf{j}^{(2)}_{ij,PS}(\mathbf{k}_i,\mathbf{k}_j)=-i(\tau_i\times\tau_j)_z\left[v_{PS}(k_j)\sigma_i(\sigma_j\cdot\mathbf{k}_j)-v_{PS}(k_i)\sigma_j(\sigma_i\cdot\mathbf{k}_i)\frac{\mathbf{k}_i-\mathbf{k}_j}{k_i^2-k_j^2}[v_{PS}(k_i)-v_{PS}(k_j)](\sigma_i\cdot\mathbf{k}_i)(\sigma_j\cdot\mathbf{k}_j)\right],\quad(3.8)$$

$$\mathbf{j}^{(2)}_{ij,V}(\mathbf{k}_i,\mathbf{k}_j)=-i(\tau_i\times\tau_j)_z\left[v_V(k_j)\sigma_i\times(\sigma_j\times\mathbf{k}_j)-v_V(k_i)\sigma_j\times(\sigma_i\times\mathbf{k}_i)-\frac{v_V(k_i)-v_V(k_j)}{k_i^2-k_j^2}\right.$$

$$\left.\times[(\mathbf{k}_i-\mathbf{k}_j)(\sigma_i\times\mathbf{k}_i)\cdot(\sigma_j\times\mathbf{k}_j)+(\sigma_i\times\mathbf{k}_i)\sigma_j\cdot(\mathbf{k}_i\times\mathbf{k}_j)+(\sigma_j\times\mathbf{k}_j)\sigma_i\cdot(\mathbf{k}_i\times\mathbf{k}_j)]+\frac{\mathbf{k}_i-\mathbf{k}_j}{k_i^2-k_j^2}[v_{VS}(k_i)-v_{VS}(k_j)]\right],$$

$$(3.9)$$

where $\mathbf{q}=\mathbf{k}_i+\mathbf{k}_j$, and $v_{PS}(k)$, $v_V(k)$, and $v_{VS}(k)$ are related to the Fourier transforms of the radial functions $v^{\sigma\tau}(r)$, $v^{t\tau}(r)$, and $v^{c\tau}(r)$, as defined in Appendix A, by

$$v_{PS}(k)=2v^{t\tau}(k)-v^{\sigma\tau}(k),\qquad(3.10)$$

$$v_V(k)=v^{t\tau}(k)+v^{\sigma\tau}(k),\qquad(3.11)$$

$$v_{VS}(k)=v^{c\tau}(k).\qquad(3.12)$$

In a one-boson-exchange (OBE) interaction model, in which the isospin-dependent central, spin-spin, and tensor components are due to π and ρ exchanges, $v_{PS}(k)$, $v_V(k)$, and $v_{VS}(k)$ are given by

$$v_{PS}(k)\rightarrow\frac{f_\pi^2}{m_\pi^2}\frac{1}{k^2+m_\pi^2},\qquad(3.13)$$

$$v_V(k)\rightarrow-\frac{g_\rho^2}{4m^2}\frac{(1+\kappa)^2}{k^2+m_\rho^2},\qquad(3.14)$$

$$v_{VS}(k)\rightarrow g_\rho^2\frac{1}{k^2+m_\rho^2},\qquad(3.15)$$

where m_π and m_ρ are the meson masses, f_π, g_ρ, and κ are the pseudovector πNN, the vector and tensor ρNN coupling constants ($f_\pi^2/4\pi=0.075$, $g_\rho^2/4\pi=0.55$, and $\kappa=6.6$), respectively. The resulting $\mathbf{j}^{(2)}_{ij,PS}$ and $\mathbf{j}^{(2)}_{ij,V}$ (suitably modified by the inclusion of form factors at the πNN and ρNN vertices) then have the standard forms commonly used in the literature [3,18,43]. The Argonne v_{14} and v_{18} interactions are not strictly OBE models. However, the $v_{PS}(k)$, $v_V(k)$, and $v_{VS}(k)$ components, projected out from the $v^{c\tau}$, $v^{\sigma\tau}$, and $v^{t\tau}$ interactions, are quite similar to those due to π and ρ exchanges [24]. This is illustrated in Fig. 2 for the $v_{PS}(k)$ component, associated to which is the leading MI current operator.

Additional but far less important MI two-body currents are obtained from the momentum-dependent terms of the interaction. They are predominantly isoscalar and give small contributions to the magnetic moment and structure function $B(q)$ of the deuteron [25,30], and to the isoscalar combination of the magnetic moments and form factors of the trinucleons [24,29].

IV. CROSS SECTION AND POLARIZATION OBSERVABLES

A. Definitions

In the center of mass (c.m.) frame, the radiative transition amplitude between an initial dN continuum state with deuteron and nucleon spin projections σ_2 and σ, respectively, and relative momentum $\mathbf{p}$, and a final trinucleon bound state with spin projection σ_3 is given by
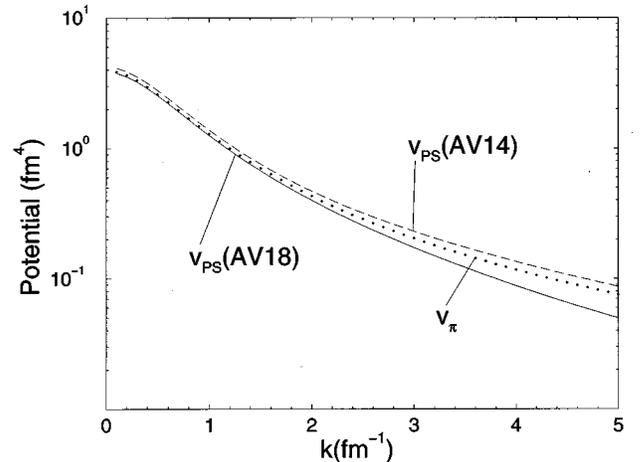

FIG. 2. The pseudoscalar components of the Argonne v_{14} (AV14) and v_{18} (AV18) interactions are compared with the one-pion-exchange potential, Eq. (3.13).

$$j_{\sigma_3\sigma_2\sigma}^{\lambda}(\mathbf{p},\mathbf{q})=\langle\Psi_3^{(1/2)\sigma_3}|\hat{\epsilon}_\lambda^*(\mathbf{q})\cdot\mathbf{j}^\dagger(\mathbf{q})|\Psi_{\mathbf{p},\sigma_2\sigma}^{(+)}\rangle,\quad(4.1)$$

where $\epsilon_\lambda(\mathbf{q})$, $\lambda=\pm1$, are the spherical components of the photon polarization vector. For a dp state the wave function $\Psi^{(+)}$ is related to the wave functions $\Psi_{2+1}^{JJ_zLS}$ introduced in Sec. II via

$$\Psi_{\mathbf{p},\sigma_2\sigma}^{(+)}=4\pi\sum_{SS_z}\langle\tfrac{1}{2}\sigma,1\sigma_2|SS_z\rangle$$
$$\times\sum_{LMJJ_z}i^L\langle SS_z,LM|JJ_z\rangle Y_{LM}^*(\hat{\mathbf{p}})\bar{\Psi}_{2+1}^{LSJJ_z},$$
$$(4.2)$$

$$\bar{\Psi}_{2+1}^{LSJJ_z}=e^{i\sigma_L}\sum_{L'S'}[1-i^JR]_{LS,L'S'}^{-1}\Psi_{2+1}^{L'S'JJ_z},\quad(4.3)$$

where σ_L is the Coulomb phase shift. For a dn state the factor $e^{i\sigma_L}$ is omitted. The wave function $\Psi^{(+)}$ satisfies outgoing wave boundary conditions, and is normalized to unit flux, while the two- and three-nucleon bound-state wave functions are normalized to one.

The cross section and polarization observables are easily obtained from the transition matrix elements $j_{\sigma_3\sigma_2\sigma}^\lambda(\mathbf{p},\mathbf{q})$.

The unpolarized differential cross section is written as

$$\sigma_u(\theta)=\frac{1}{6}\sigma_0\sum_{\lambda\sigma_3\sigma_2\sigma}|j_{\sigma_3\sigma_2\sigma}^\lambda(\mathbf{p},\mathbf{q})|^2,\quad(4.4)$$

where the factor 1/6 comes from the average over the initial state polarizations, θ is the angle between $\mathbf{p}$ and $\mathbf{q}$ (the vectors $\mathbf{p}$ and $\mathbf{q}$ define the xz plane), and

$$\sigma_0=\frac{1}{8\pi^2v_{\rm rel}}\frac{q}{1+q/m_3}.\quad(4.5)$$

Here $v_{\rm rel}$ is the dN relative velocity and m_3 the mass of the trinucleon. The c.m. energy of the emitted γ ray is given by

$$q=\frac{B_3-B_2+p^2/2\mu}{[\sqrt{1-2(B_3-B_2+p^2/2\mu)/m_3}+1]/2},\quad(4.6)$$

where B_2 and B_3 are the binding energies of the deuteron and trinucleon. The differential cross section $\sigma_{fi}(\theta)$ for a process in which an initial state with polarization defined by the density matrix ρ_i leads to a final polarization state with density matrix ρ_f, can be expressed as

$$\sigma_{fi}(\theta)=4\sigma_0\sum_{\lambda\sigma_3\sigma_2\sigma}\sum_{\lambda'\sigma_3'\sigma_2'\sigma'}[j_{\sigma_3\sigma_2\sigma}^\lambda(\mathbf{p},\mathbf{q})](\rho_i)_{\sigma_2\sigma,\sigma_2'\sigma'}[j_{\sigma_3'\sigma_2'\sigma'}^{\lambda'}(\mathbf{p},\mathbf{q})]^*(\rho_f)_{\lambda'\sigma_3',\lambda\sigma_3}.\quad(4.7)$$

The initial density matrix is given by the product of the nucleon and deuteron density matrices:

$$(\rho_i)_{\sigma_2\sigma,\sigma_2'\sigma'}^{[\mathbf{P}_N,P_d^{\lambda\mu}]}=\frac{1}{2}[1+\sigma\cdot\mathbf{P}_p]_{\sigma,\sigma'}\frac{1}{3}\left[\sum_{\lambda\mu}P_d^{\lambda\mu}t^{\lambda\mu}\right]_{\sigma_2,\sigma_2'},\quad(4.8)$$

where $\mathbf{P}_N$ and $P_d^{\lambda\mu}$ are the polarizations of the spin-1/2 nucleon and spin-1 deuteron beams, respectively. The matrices $t^{\lambda\mu}$ are defined as

$$t_{\sigma_2\sigma_2'}^{\lambda\mu}=\sqrt{3}\sum_{\sigma_2\sigma_2'}(-)^{1-\sigma_2}\langle1\sigma_2',1-\sigma_2|\lambda\mu\rangle.\quad(4.9)$$

For example, an unpolarized deuteron beam has $P_d^{\lambda\mu}=\delta_{\lambda0}\delta_{\mu0}$. Since in the final state we are interested in processes for which only the polarization of the emitted photon is detected, ρ_f can be written as

$$(\rho_f)_{\lambda\sigma_3,\lambda'\sigma_3'}^{[P_\ell,P_c]}=\frac{1}{2}[\delta_{\lambda,\lambda'}+P_\ell\delta_{\lambda,-\lambda'}+\lambda P_c\delta_{\lambda,\lambda'}]\frac{1}{2}\delta_{\sigma_3,\sigma_3'},\quad(4.10)$$

where P_ℓ (P_c) is the linear (circular) polarization of the emitted photon. Note that $P_\ell=P_y-P_x$.

With the density matrices given in Eqs. (4.8) and (4.10) the initial and final state polarizations are defined by assigning the quantities $\mathbf{P}_N$, $P_d^{\lambda\mu}$, P_ℓ, and P_c. Polarization observables are then obtained from differences of cross sections

$$\sigma_{fi}(\theta)\equiv\sigma(\theta;\mathbf{P}_N,P_d^{\lambda\mu},P_\ell,P_c).\quad(4.11)$$

Thus the proton and deuteron vector and tensor analyzing powers $A_y(\theta)$ and $T_{20}(\theta)$ are given, respectively, by

$$\sigma_u(\theta)A_y(\theta)=\frac{1}{2}[\sigma(\theta;\mathbf{P}_N=\hat{\mathbf{y}},\delta_{\lambda0}\delta_{\mu0},0,0)$$
$$-\sigma(\theta;\mathbf{P}_N=-\hat{\mathbf{y}},\delta_{\lambda0}\delta_{\mu0},0,0)],\quad(4.12)$$

$$\sigma_u(\theta)T_{20}(\theta)=\frac{1}{2}[\sigma(\theta;0,+\delta_{\lambda2}\delta_{\mu0},0,0)$$
$$-\sigma(\theta;0,-\delta_{\lambda2}\delta_{\mu0},0,0)].\quad(4.13)$$

Expressions for more complicated double polarization observables are obtained in similar fashion. The photon linear polarization coefficient $P_\gamma(\theta)$ is defined as

$$\sigma_u(\theta)P_\gamma(\theta)=\frac{1}{2}[\sigma_\parallel(\theta)-\sigma_\perp(\theta)],\quad(4.14)$$

where

$$\sigma_{\perp}(\theta) = \sigma(\theta; 0, \delta_{\lambda 0} \delta_{\mu 0}, P_{\ell} = 1, 0), \qquad (4.15)$$

$$\sigma_{\parallel}(\theta) = \sigma(\theta; 0, \delta_{\lambda 0} \delta_{\mu 0}, P_{\ell} = -1, 0). \qquad (4.16)$$

Here $\sigma_{\parallel}(\theta)$ $[\sigma_{\perp}(\theta)]$ corresponds to a capture cross section in which an unpolarized initial state leads to emission of a photon with polarization parallel (perpendicular) to the reaction plane. The observation of circular polarization $P_{\Gamma}(\theta)$,

$$\sigma_u(\theta) P_{\Gamma}(\theta) = \frac{1}{2} [\sigma(\theta; \mathbf{P}_N, \delta_{\lambda 0} \delta_{\mu 0}, 0, P_c = 1)$$
$$- \sigma(\theta; \mathbf{P}_N, \delta_{\lambda 0} \delta_{\mu 0}, 0, P_c = -1)],$$
$$(4.17)$$

requires the polarization of the initial proton (or neutron) beam. If the process is dominated by S-wave capture, as is the case for the ${}^2\mathrm{H}(n, \gamma){}^3\mathrm{H}$ reaction at thermal neutron energies, then $P_{\Gamma}(\theta)$ is simply given by

$$P_{\Gamma}(\theta) = R_c \mathbf{P}_N \cdot \hat{\mathbf{q}} \quad (S\text{-wave capture only}), \quad (4.18)$$

where R_c is the so-called polarization parameter.

B. Expressions in terms of electric and magnetic multipoles

The expansion of the transition matrix element $j^{\lambda}_{\sigma_3 \sigma_2 \sigma}(\mathbf{p}, \mathbf{q})$ in terms of electric and magnetic multipoles, $E^{LSJ}_{\ell}(q)$ and $M^{LSJ}_{\ell}(q)$, respectively, is given by [44]

$$j^{\lambda}_{\sigma_3 \sigma_2 \sigma}(\mathbf{p}, \mathbf{q}) = 2\pi \sum_{LSJJ_z \ell m} \hat{\ell} \hat{L} i^L (-i)^{\ell} \langle \tfrac{1}{2}\sigma, 1\sigma_2 | SJ_z \rangle \langle SJ_z, L0 | JJ_z \rangle \langle JJ_z, \ell m | \tfrac{1}{2}\sigma_3 \rangle \mathcal{D}^{\ell}_{m, -\lambda}(0, \theta, 0) [-\lambda M^{LSJ}_{\ell}(q) - E^{LSJ}_{\ell}(q)],$$
$$(4.19)$$

where $\mathcal{D}^{\ell}_{m, -\lambda}$ are standard rotation matrices [45], and $\hat{L} \equiv \sqrt{2L + 1}$ and similarly for $\hat{\ell}$. The angle θ is defined as that between the $\mathbf{p}$ direction (which is also taken as the quantization axis of the initial and final nuclear spins) and the $\mathbf{q}$ direction. We have adopted a different spin coupling order between the channel spin and orbital angular momentum of the initial state with respect to that used in Ref. [46]. Regarding the choice of phase between the electric and magnetic multipole components of the transverse vector potential, our definition is equivalent to the choice of the positive sign in Eq. (17) of Ref. [46].

By evaluating the sums in Eqs. (4.4) and (4.7), and using the product property of the $\mathcal{D}$ matrices, the angular dependence of the unpolarized cross section as well as that of the vector and tensor analyzing powers and photon linear coefficient of interest in the present study are made explicit [46]:

$$\sigma_u(\theta) = \sum_{k \geq 0} a_k P_k(\cos\theta), \qquad (4.20)$$

$$\sigma_u(\theta) A_y(\theta) = \sum_{k \geq 1} b_k P^1_k(\cos\theta), \qquad (4.21)$$

$$\sigma_u(\theta) T_{20}(\theta) = \sum_{k \geq 0} c_k P_k(\cos\theta), \qquad (4.22)$$

$$\sigma_u(\theta) P_{\gamma}(\theta) = \sum_{k \geq 2} d_k P^2_k(\cos\theta), \qquad (4.23)$$

where P_k (P^m_k) are Legendre polynomials (associated Legendre functions), and the coefficients a_k, b_k, c_k, and d_k denote appropriate combinations of electric and magnetic multipoles. Expressions for the leading coefficients in the expansions above for each of the observables considered here are listed in Appendix B of the present work.

V. CALCULATION

In this section we discuss the evaluation of the electric and magnetic multipole matrix elements. By using the partial wave decomposition of the wave function $\Psi^{(+)}$ in Eq. (4.2), we write

$$j^{\lambda}_{\sigma_3 \sigma_2 \sigma}(\mathbf{p}, \mathbf{q}) = 4\pi \sum_{SS_z} \langle \tfrac{1}{2}\sigma, 1\sigma_2 | SS_z \rangle \sum_{LMJJ_z} i^L \langle SS_z, LM | JJ_z \rangle Y^*_{LM}(\hat{\mathbf{p}}) j^{LSJJ_z}_{\lambda \sigma_3}(\mathbf{q}), \qquad (5.1)$$

where

$$j^{LSJJ_z}_{\lambda \sigma_3}(\mathbf{q}) = \langle \Psi^{(1/2)\sigma_3}_3 | \hat{\epsilon}^*_{\lambda}(\mathbf{q}) \cdot \mathbf{j}^{\dagger}(\mathbf{q}) | \bar{\Psi}^{LSJJ_z}_{2+1} \rangle. \qquad (5.2)$$

In a frame where the $\mathbf{q}$ direction also defines the quantization axis for the nuclear spins, the matrix element $j^{LSJJ_z}_{\lambda \sigma_3}$ has the multipole expansion [44]

$$j_{\lambda\sigma_3}^{LSJJ_z}(q)=\sqrt{\pi}\sum_{\ell=1}^{\infty}\hat{\ell}(-i)^{\ell}\langle JJ_z,\ell-\lambda|\tfrac{1}{2}\sigma_3\rangle[-\lambda M_{\ell}^{LSJ}(q)-E_{\ell}^{LSJ}(q)].\tag{5.3}$$

We note that the expansion above is different from that given in Eq. (4.19), since in the latter the quantization axis for the nuclear spins was taken as that defined by the relative momentum **p** direction, and **q** made an angle θ with **p**.

Using Eq. (5.3), the E_{ℓ}^{LSJ} and M_{ℓ}^{LSJ} are obtained from linear combinations of the $j_{\lambda\sigma_3}^{LSJJ_z}$ matrix elements. We find, for example,

$$M_1^{0(1/2)(1/2)}(q)=\frac{i}{\sqrt{2\pi}}j_{-1(1/2)}^{0(1/2)(1/2)-(1/2)}(q),\tag{5.4}$$

$$M_1^{0(3/2)(3/2)}(q)=\frac{i}{2\sqrt{2\pi}}[j_{-1(1/2)}^{0(3/2)(3/2)-(1/2)}(q)$$
$$-\sqrt{3}j_{+1,(1/2)}^{0(3/2)(3/2)(3/2)}(q)].\tag{5.5}$$

The problem is now reduced to the evaluation of the $j_{\lambda\sigma_3}^{LSJJ_z}$ matrix elements, which we write schematically as

$$j_{fi}=\frac{\langle\Psi_f|j|\Psi_i\rangle}{[\langle\Psi_f|\Psi_f\rangle\langle\Psi_i|\Psi_i\rangle]^{1/2}}.\tag{5.6}$$

The initial and final states $|\Psi_x\rangle$ ($x=i$ or f) have the form of Eq. (2.11). It is convenient to expand these as [23]

$$|\Psi_x\rangle=\Psi_N^x+\sum_{i<j}U_{ij}^{TR}\Psi_N^x+\cdots\tag{5.7}$$

and the matrix element of the current operator becomes

$$\langle\Psi_f|j|\Psi_i\rangle=\langle\Psi_N^f|j(N\ \text{only})|\Psi_N^i\rangle+\langle\Psi_N^f|j(\Delta)|\Psi_N^i\rangle,\tag{5.8}$$

where $j(N\ \text{only})$ denotes all one- and two-body contributions to **j**(**q**) which only involve nucleon degrees of freedom, i.e., $j(N\ \text{only})=j^{(1)}(N\rightarrow N)+j^{(2)}(NN\rightarrow NN)$. The operator $j(\Delta)$ includes terms involving the Δ-isobar degrees of freedom, coming from the explicit Δ currents $j^{(1)}(N\rightarrow\Delta)$, $j^{(1)}(\Delta\rightarrow N)$, and $j^{(1)}(\Delta\rightarrow\Delta)$, and the transition operators U_{ij}^{TR} The operator $j(\Delta)$ is illustrated in Fig. 3. The terms in Figs. 3(a)–3(g) are two-body current operators. Those in Figs. 3(h)–3(l) are to be interpreted as normalization corrections to the ''nucleonic'' matrix elements $\langle\Psi_N^f|j(N\ \text{only})|\Psi_N^i\rangle$, due to the presence of Δ-isobar components in the wave functions. We note that not included in $j(\Delta)$ are all remaining connected three-body contributions of the type shown in Fig. 4. These are neglected in the present work, since they are expected to be significantly smaller than those considered in Fig. 3.

Each of the terms in Fig. 3 is expressed as an operator acting on the nucleon coordinates. For example, the terms in Figs. 3(a) and 3(b) have the structure [23]

$$\sum_{ij}j_i(\Delta\rightarrow N)U_{ij}^{\Delta N}+U_{ij}^{\Delta N\dagger}j_i(N\rightarrow\Delta),\tag{5.9}$$

which can easily be reduced to operators involving only Pauli spin and isospin matrices by use of the identity

$$\mathbf{S}^{\dagger}\cdot\mathbf{AS}\cdot\mathbf{B}=\frac{2}{3}\mathbf{A}\cdot\mathbf{B}-\frac{i}{3}\sigma\cdot(\mathbf{A}\times\mathbf{B}),\tag{5.10}$$

where **A** and **B** are vector operators that commute with σ, but not necessarily with each other. Expressions for the other terms in Fig. 3 are obtained in a similar fashion [23].

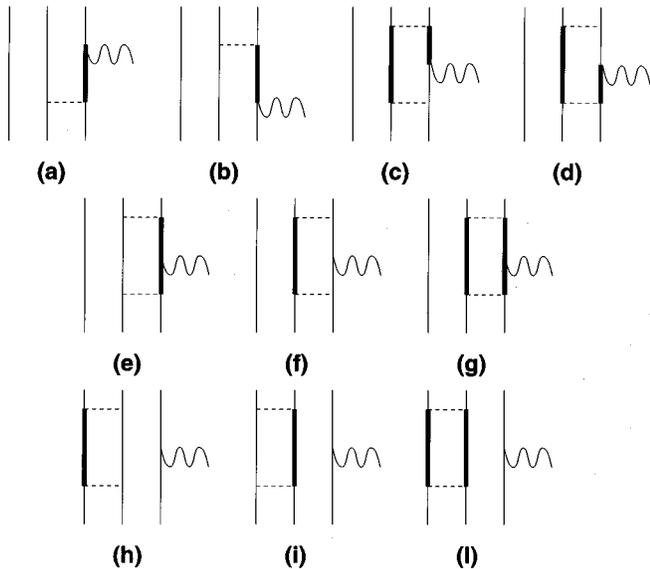The normalization of the wave function is given by [23]

FIG. 3. Diagrams included in $j(\Delta)$. Wavy, thin, thick, and dashed lines denote photons, nucleons, Δ isobars, and transition correlations U_{ij}^{TR} respectively.
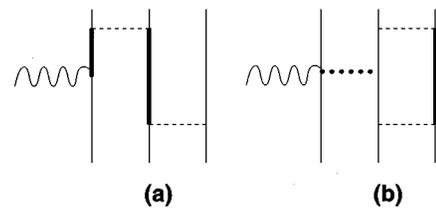

FIG. 4. Diagrams associated with connected three-body terms, which are neglected in the present work. Wavy, thin, thick, and dashed lines denote photons, nucleons, Δ isobars, and transition correlations U_{ij}^{TR} respectively, while the dotted line represents all two-body current contributions included in $\mathbf{j}_{ij}^{(2)}$.

$$\langle\Psi|\Psi\rangle=\langle\Psi_N|\Psi_N\rangle+\left\langle\Psi_N\left|\sum_{i<j}\left[2\,U_{ij}^{\Delta N\dagger}U_{ij}^{\Delta N}+U_{ij}^{\Delta\Delta\dagger}U_{ij}^{\Delta\Delta}\right]\right|\Psi_N\right\rangle+\text{(three-body terms)},\qquad(5.11)$$

and the three-body terms have been neglected consistently with the approximation introduced in Eq. (5.8).

The matrix elements in Eqs. (5.8) and (5.11) are computed by Monte Carlo integration. The wave functions are written as vectors in the spin-isospin space of the three nucleons for any given spatial configuration $\mathbf{R}=\{\mathbf{r}_1,\mathbf{r}_2,\mathbf{r}_3\}$. For the given $\mathbf{R}$, we calculate the state vector $[j(N\ \text{only})+j(\Delta)]|\Psi_N^f\rangle$ by performing exactly the spin-isospin algebra with the techniques described in Refs. [24,47]. The spatial integrations are carried out with the Monte Carlo method by sampling the $\mathbf{R}$ configurations according to the Metropolis algorithm [48]. Finally, we note that the statistical errors in the Monte Carlo evaluation of matrix elements of the type $\langle\Psi^{(1/2)\sigma_3}|\hat{\epsilon}^*(\mathbf{q})\cdot\mathbf{j}^\dagger(\mathbf{q})|\bar{\Psi}_{2+1}^{0(1/2)(1/2)J_z}\rangle$ are significantly reduced by explicitly enforcing the orthogonality between the initial dN S-wave doublet continuum state and the final trinucleon bound state, namely

$$|\bar{\Psi}_{2+1}^{0(1/2)(1/2)J_z}\rangle\rightarrow|\bar{\Psi}_{2+1}^{0(1/2)(1/2)J_z}\rangle$$

$$-\sum_{\sigma_3'}|\Psi_3^{(1/2)\sigma_3'}\rangle\langle\Psi_3^{(1/2)\sigma_3'}|\bar{\Psi}_{2+1}^{0(1/2)(1/2)J_z}\rangle.$$

$$(5.12)$$

VI. RESULTS

In this section we present our estimates for the cross section and photon polarization parameter of the thermal neutron radiative capture on ^{2}H, and for the S-factor, vector and tensor analyzing powers, and photon linear polarization coefficient of the ^{2}H$(\vec{p},\gamma)^3$He and $p(\vec{d},\gamma)^3$He reactions in the center of mass energy range 0–100 keV. In Table II we give the results for the two- and three-body bound-state wave function normalizations $\langle\Psi|\Psi\rangle/\langle\Psi_N|\Psi_N\rangle$.

In Tables III–VIII, the impulse-approximation (IA) results have been obtained by using the ''nucleonic'' one-body current in Eq. (3.3), while the IA+PS results include in addition the leading two-body current contribution associated with the ''model-independent'' (MI) $\mathbf{j}_{PS}$ term, Eq. (3.8). The IA+MI and IA+MI+MD results correspond to calculations in which, respectively, only the MI and both the MI and ''model-dependent'' (MD) two-body current contributions are included (in addition to the IA contribution). Finally, the IA+$\cdots$+Δ results correspond to the complete calculations including Δ-isobar components in the nuclear wave function.

In these tables as well as in Figs. 7–11, the cumulative nucleonic contributions are normalized as

$$[\text{IA}+\cdots+\text{MD}]=\frac{\langle\Psi_N^f|j(N\ \text{only})|\Psi_N^i\rangle}{[\langle\Psi_N^f|\Psi_N^f\rangle\langle\Psi_N^i|\Psi_N^i\rangle]^{1/2}}.\qquad(6.1)$$

However, when the isobaric contributions are added to the cumulative sum, the normalization changes to

$$[\text{IA}+\cdots+\Delta]=\frac{\langle\Psi_f|j(N\ \text{only})+j(\Delta)|\Psi_i\rangle}{[\langle\Psi_f|\Psi_f\rangle\langle\Psi_i|\Psi_i\rangle]^{1/2}}.\qquad(6.2)$$

In the previous equations, the normalization of the initial scattering state is the same as that of d, up to corrections of order (volume)$^{-1}$.

We also report results, denoted with IA+$\cdots$+Δ_{PT}, in which the Δ components in the nuclear wave functions are treated in perturbation theory, as discussed in Sec. II D, and the $j(\Delta)$ only includes the operators in Figs. 3(a) and 3(b) (in fact, this approach is most commonly used to study the effect of Δ degrees of freedom in nuclei [3,18]). In this case, the cumulative contributions [IA+$\cdots$+Δ_{PT}] are normalized as in Eq. (6.1).

As already mentioned in Sec. IV, three-body terms have not been retained in the evaluation of either the matrix elements $\langle\Psi_f|j(\Delta)|\Psi_i\rangle$ or the normalization, Eq. (5.11), as they are expected to provide a small correction [23].

A. Thermal nd radiative capture

At thermal energies the reaction proceeds through S-wave capture predominantly via magnetic dipole transitions $M_1^{0(1/2)(1/2)}$ and $M_1^{0(3/2)(3/2)}$ from the initial doublet $J=1/2$ and quartet $J=3/2$ dn scattering states. In addition, there is a small contribution due to an electric quadrupole transition $E_2^{0(3/2)(3/2)}$ from the initial quartet state.

The calculations have been carried out with wave functions obtained from the AV14/VIII and AV18/IX Hamiltonian models. The calculated values for the $\widetilde{M}_1^{0(1/2)(1/2)}$, $\widetilde{M}_1^{0(3/2)(3/2)}$, and $\widetilde{E}_2^{0(3/2)(3/2)}$ reduced matrix elements (RME's), which are related to those defined in Eq. (5.3) via

$$\widetilde{X}_\ell^{LSJ}=\frac{\sqrt{6\pi}}{q\mu_N}\sqrt{4\pi}X_\ell^{LSJ},\qquad(6.3)$$

are listed in Table III. Here, X stands for either E or M, and μ_N is nuclear magneton. In terms of the $\widetilde{X}_\ell^{LSJ}$ RME, the total cross section is given by

$$\sigma_T=\frac{2}{9}\frac{\alpha}{v_{\text{rel}}}\frac{q^3}{4m^2}\sum_{\ell LSJ}|\widetilde{E}_\ell^{LSJ}|^2+|\widetilde{M}_\ell^{LSJ}|^2,\qquad(6.4)$$

where $\alpha=e^2/4\pi$.

Inspection of Table III shows the following.

TABLE II. The wave function normalization ratios $\langle\Psi|\Psi\rangle/\langle\Psi_N|\Psi_N\rangle$ for the two- and three-body systems.

Hamiltonian	^{2}H	^{3}H
AV14/VIII	1.004	1.024
AV18/IX	1.004	1.025

TABLE III. Reduced matrix elements (RME's) in fm$^{3/2}$ calculated with the AV14/VIII and AV18/IX Hamiltonian models for the ^{2}H(n,γ) ^{3}H reaction at thermal energies. See text for notation. Note that the M_1 RME's are purely imaginary, whereas the E_2 RME is purely real. The statistical errors associated with the Monte Carlo integrations are less than 1% for the M_1 RME, and about 10% for the E_2 RME.

| | AV14/VIII | | | AV18/IX | | |
	$\widetilde{M}_1^{0(1/2)(1/2)}$	$\widetilde{M}_1^{0(3/2)(3/2)}$	$\widetilde{E}_2^{0(3/2)(3/2)}$	$\widetilde{M}_1^{0(1/2)(1/2)}$	$\widetilde{M}_1^{0(3/2)(3/2)}$	$\widetilde{E}_2^{0(3/2)(3/2)}$
IA	−10.7	13.2	−1.3	−10.7	13.4	−0.17
IA+PS	−19.3	12.4	−1.0	−18.3	12.6	−0.16
IA+MI	−22.2	12.3	−1.0	−21.6	12.6	−0.13
IA+MI+MD	−22.5	12.1	−1.0	−21.8	12.5	−0.14
IA+$\cdots$+Δ_{PT}	−26.6	11.6	−1.0	−25.9	12.0	−0.14
IA+$\cdots$+Δ	−25.1	11.8	−1.0	−24.4	12.2	−0.14

(1) As expected, the electric quadrupole (E_2) RME is much smaller, in absolute value, than both the doublet and quartet magnetic dipole (M_1) RME.

(2) In IA the quartet M_1 RME is, in absolute value, about 23% larger than the doublet M_1. However, two-body current and Δ degrees of freedom contributions (row labeled IA $+\cdots+\Delta$) are large and interfere constructively with the IA contribution for the doublet M_1, while they are much smaller and interfere destructively with the IA contribution for the quartet M_1. Consequently, the IA$+\cdots+\Delta$ doublet M_1 is found to be larger than the quartet M_1 by more than a factor of 2.

(3) In IA both the doublet and quartet M_1 RME are found to be rather insensitive to the Hamiltonian model used; however, in the IA+PS calculation, the AV14/VIII prediction for the doublet M_1 RME is, in absolute value, about 5% larger than that obtained with the AV18/IX Hamiltonian. The v_{18} has a weaker tensor force than the v_{14}, leading to a weaker PS current (the dominant two-body current). However, the AV14/VIII result for the doublet M_1 RME is only 3% larger than the AV18/IX result in the approximation IA$+\cdots+\Delta$.

(4) The predicted values for the E_2 RME, in contrast to those for the M_1 RME, are found to be very sensitive to the Hamiltonian model used, even in IA. The reason for such sensitivity is discussed below.

The results for the cross section and photon polarization parameter are presented in Table IV, along with the experimental data. The cross section in IA is calculated to be approximately a factor of 2 smaller than the measured value, while the IA$+\cdots+\Delta$ calculations based on the AV14/VIII

and AV18/IX Hamiltonians overestimate the experimental value by 18 and 14 %, respectively. It should be noted, however, that the common perturbative treatment of Δ-isobar degrees of freedom (row labeled IA$+\cdots+\Delta_{PT}$) leads to a significant increase of the discrepancy between theory and experiment.

The photon polarization parameter is very sensitive to two-body currents. For example, for the AV18/IX Hamiltonian their inclusion produces roughly a sixfold increase, in absolute value, of the IA prediction (rows labeled IA and IA+MI+MD in Table IV). Contributions associated with Δ components in the nuclear wave functions lead only to a further 7% increase (absolute value) of the IA+MI+MD results. More interesting is the sensitivity displayed by R_c to the small E_2 RME, particularly for the AV14/VIII Hamiltonian. In S-wave capture this matrix element is predominantly due to transitions $S(^2$H$)\rightarrow D(^3$H$)$ and $D(^2$H$)\rightarrow S(^3$H$)$, where S and D denote S- and D-wave components in the bound-state wave functions. In the case of the AV18/IX Hamiltonian, the contributions associated with these transitions interfere destructively, thus producing a small E_2 RME; in contrast, for the AV14/VIII Hamiltonian the interference between these contributions is constructive. This is most clearly seen by considering the function $\widetilde{E}_2^{0(3/2)(3/2)}(q;r_{dn})$ such that

$$\widetilde{E}_2^{0(3/2)(3/2)}(q) = \int_0^\infty dr_{dn} \widetilde{E}_2^{0(3/2)(3/2)}(q;r_{dn}), \quad (6.5)$$

where r_{dn} is the dn relative distance. This function is easily

TABLE IV. Cumulative contributions to the cross section (in mb) and photon polarization parameter R_c of the reaction ^{2}H(n,γ) ^{3}H at thermal energies calculated with the AV14/VIII and AV18/IX Hamiltonian models. $R_c(M_1)$ [$R_c(M_1+E_2)$] has been calculated without (with) inclusion of the electric quadrupole contribution. See text for notation. The statistical errors associated with the Monte Carlo integrations are less than 2%. The experimental values for σ_T and R_c are from Refs. [5,8], respectively.

| | σ_T | | $R_c(M_1)$ | | $R_c(M_1+E_2)$ | |
	AV14/VIII	AV18/IX	AV14/VIII	AV18/IX	AV14/VIII	AV18/IX
IA	0.225	0.229	−0.089	−0.083	0.029	−0.068
IA+PS	0.409	0.383	−0.422	−0.397	−0.345	−0.385
IA+MI	0.502	0.481	−0.460	−0.446	−0.389	−0.437
IA+MI+MD	0.509	0.489	−0.464	−0.452	−0.394	−0.442
IA+$\cdots$+Δ_{PT}	0.658	0.631	−0.492	−0.487	−0.430	−0.478
IA+$\cdots$+Δ	0.600	0.578	−0.485	−0.477	−0.420	−0.469
Expt.	0.508±0.015				−0.42±0.03	

THEORETICAL STUDY OF THE RADIATIVE CAPTURE . . .

TABLE V. RME in fm$^{3/2}$ calculated with the AV14/VIII and AV18/IX Hamiltonian models for the reaction ^{2}H$(p,\gamma)^3$He at zero energy. See text for notation. Note that the M_1 and M_2 RME's are purely imaginary, whereas the E_1 and E_2 RME's are purely real. The statistical errors associated with the Monte Carlo integrations are less than 1% for the M_1 and doublet E_1 RME, about 5% for the quartet E_1 RME, and of the order of 10 (50) % for the E_2 (M_2) RME.

	IA	IA+PS	IA+MI	IA+MI+MD	IA+$\cdots$+Δ_{PT}	IA+$\cdots$+Δ
				AV14/VIII		
$\widetilde{M}_{1C}^{0(1/2)(1/2)}$	−18.7	−30.4	−32.7	−33.6	−39.1	−36.1
$\widetilde{M}_{1C}^{0(3/2)(3/2)}$	27.2	25.7	24.9	25.0	24.1	24.4
$\widetilde{E}_{2C}^{0(3/2)(3/2)}$	0.86	1.12	1.07	1.08	1.08	1.06
$\widetilde{E}_{1C}^{1(1/2)(1/2)}$	−19.2	−19.7	−20.2	−20.2	−20.2	−19.9
$\widetilde{E}_{1C}^{1(3/2)(1/2)}$	−1.30	5.85	4.21	4.27	4.27	4.20
$\widetilde{E}_{1C}^{1(1/2)(3/2)}$	28.3	31.5	32.4	32.4	32.4	31.9
$\widetilde{E}_{1C}^{1(3/2)(3/2)}$	−0.01	3.73	3.07	3.10	3.11	3.06
$\widetilde{M}_{2C}^{0(1/2)(3/2)}$	−0.14	−0.14	−0.12	−0.12	−0.12	−0.12
$\widetilde{M}_{2C}^{0(3/2)(3/2)}$	0.20	0.20	0.19	0.19	0.19	0.19
				AV18/IX		
	IA	IA+PS	IA+MI	IA+MI+MD	IA+$\cdots$+Δ_{PT}	IA+$\cdots$+Δ
$\widetilde{M}_{1C}^{0(1/2)(1/2)}$	−19.4	−30.1	−32.1	−32.9	−38.4	−35.4
$\widetilde{M}_{1C}^{0(3/2)(3/2)}$	28.1	26.7	25.9	25.9	25.1	25.3
$\widetilde{E}_{2C}^{0(3/2)(3/2)}$	0.85	1.10	1.06	1.07	1.07	1.05
$\widetilde{E}_{1C}^{1(1/2)(1/2)}$	−21.1	−21.8	−22.2	−22.2	−22.2	−21.7
$\widetilde{E}_{1C}^{1(3/2)(1/2)}$	−1.27	5.32	3.74	3.79	3.79	3.71
$\widetilde{E}_{1C}^{1(1/2)(3/2)}$	29.5	32.6	33.3	33.3	33.3	32.6
$\widetilde{E}_{1C}^{1(3/2)(3/2)}$	−0.01	3.43	2.84	2.87	2.87	2.81
$\widetilde{M}_{2C}^{0(1/2)(3/2)}$	−0.15	−0.14	−0.15	−0.15	−0.15	−0.15
$\widetilde{M}_{2C}^{0(3/2)(3/2)}$	0.26	0.28	0.28	0.29	0.29	0.28

obtained by binning the appropriate combination of $j_{\lambda\sigma_3}^{0JJJ_z}$ matrix elements as function of r_{dn} in the Monte Carlo calculation [49].

The functions $\widetilde{E}_2^{0(3/2)(3/2)}(q;r_{dn})$, as obtained in IA, are shown in Fig. 5 by the solid curves for the AV14/VIII and AV18/IX Hamiltonian models. We also show the results obtained by switching off either the deuteron or tritium D-state components. By inspecting Fig. 5, we see that for the AV18/IX model the E_2 RME results from the delicate cancellation between positive and negative contributions associated, respectively, with the deuteron and tritium D states.

However, no such cancellation is obtained for the AV14/VIII model. Thus, the E_2 RME appears to be very sensitive upon the D-state content of the two- and three-nucleon bound-state wave functions and, therefore, upon the strength of the tensor force, as reflected in the large difference between the AV14/VIII and AV18/IX predictions. It is unfortunate that, due to the large two-body current contributions affecting the photon polarization parameter, the sensitivity displayed by this observable to the E_2 RME cannot be exploited to gain information on the tensor interaction.

Finally, we note that the AV14/VIII prediction for the cross section in the approximation IA+PS+Δ_{PT} is 0.545 mb.

TABLE VI. Doublet and quartet E_1 RME in fm$^{3/2}$ calculated with the AV14 and AV14/VIII Hamiltonian models for the reaction ^{2}H$(p,\gamma)^3$He at zero energy in IA and in the approximations IA+MI and LW. See text for notation. Statistical errors associated with the Monte Carlo integrations are in the range 1–5 %.

	AV14			AV14/VIII		
	IA	IA+MI	LW	IA	IA+MI	LW
$\widetilde{E}_{1C}^{1(1/2)(1/2)}$	−24.1	−25.5	−27.7	−19.2	−20.2	−23.5
$\widetilde{E}_{1C}^{1(3/2)(1/2)}$	−0.9	4.6	3.0	−1.3	4.2	3.1
$\widetilde{E}_{1C}^{1(1/2)(3/2)}$	32.5	36.5	37.1	28.3	32.4	33.5
$\widetilde{E}_{1C}^{1(3/2)(3/2)}$	−0.6	2.5	1.3	−0.0	3.1	1.4

TABLE VII. Cumulative contributions in eV b to the S- and P-wave capture zero energy S factor of the reaction ^{2}H$(p,\gamma)^3$He calculated with the AV14/VIII and AV18/IX Hamiltonian models. See text for notation. The statistical errors associated with the Monte Carlo integrations are less than 2%. The experimental values are taken from Ref. [11].

| | S_S | | S_P | |
	AV14/VIII	AV18/IX	AV14/VIII	AV18/IX
IA	0.0605	0.0647	0.0650	0.0731
IA+PS	0.0880	0.0900	0.0794	0.0876
IA+MI	0.0939	0.0943	0.0822	0.0900
IA+MI+MD	0.0971	0.0972	0.0824	0.0901
IA+$\cdots$+Δ_{PT}	0.117	0.117	0.0824	0.0901
IA+$\cdots$+Δ	0.105	0.105	0.0800	0.0865
Expt.	0.109±0.01		0.073±0.007	

This result is about 15% smaller than that reported by Friar and collaborators [3] for the same Hamiltonian. The difference, however, is mostly due to the different value used for the $N\rightarrow\Delta$ transition magnetic moment: we use $\mu_{\gamma N\Delta}=3\mu_N$, while Friar *et al.* used $\mu_{\gamma N\Delta}=3.993\mu_N$ from the quark model. Indeed, if we use the latter value for $\mu_{\gamma N\Delta}$, our result becomes 0.630 mb, in much better agreement with that reported in Ref. [3]. As a last remark, we note that the R_c parameter, obtained in the IA+PS+Δ_{PT} approximation by only including the M_1 RME, is calculated to be -0.49, again in excellent agreement with the value obtained in Ref. [3].

B. Thermal pd radiative capture

In Tables V and VI we present the results for the zero-energy RME and in Fig. 7 and Table VII the results for the astrophysical S factor of the ^{2}H$(p,\gamma)^3$He reaction. The latter quantity is defined as

$$S(E_{\text{c.m.}})=E_{\text{c.m.}}\sigma_T(E_{\text{c.m.}})e^{2\pi\alpha/v\,\text{rel}}, \quad (6.6)$$

where $\sigma_T(E_{\text{c.m.}})$ is the total cross section. We note that in Table V, the zero-energy RME are related to those defined in Eq. (5.3) via

$$\widetilde{X}_{/C}^{LSJ}=\sqrt{\frac{v_{\text{rel}}}{2\pi\alpha}\exp(2\pi\alpha/v_{\text{rel}})}\frac{\sqrt{6\pi}}{q\mu_N}\sqrt{4\pi}X_{/}^{LSJ}. \quad (6.7)$$

The quantities $\widetilde{X}_{/C}^{LSJ}$ are easily shown to remain finite in the limit $v_{\text{rel}}\rightarrow 0$; in terms of these the S factor is written as

$$S(E_{\text{c.m.}}=0)=\frac{\pi}{9}\alpha^2\mu\frac{q^3}{4m^2}\sum_{/LSJ}|\widetilde{E}_{/C}^{LSJ}|^2+|\widetilde{M}_{/C}^{LSJ}|^2, \quad (6.8)$$

where μ is the dp reduced mass.

The predicted angular distributions of the differential cross section $\sigma_u(\theta)$, vector and tensor analyzing powers $A_y(\theta)$ and $T_{20}(\theta)$, and photon linear polarization coefficient $P_\gamma(\theta)$, obtained for the ^{2}H$(\vec{p},\gamma)^3$He and ^{1}H$(\vec{d},\gamma)^3$He reactions are compared with the experimental data of [11] in Figs. 8–11. The calculations are based on the AV18/IX Hamiltonian. For selected observables, however, results corresponding to the AV14/VIII Hamiltonian will also be shown. The observed linear dependence upon the energy of the S factor and the observed angular distributions of $\sigma_u(\theta)$, $A_y(\theta)$, $T_{20}(\theta)$, and $P_\gamma(\theta)$ indicate that the reaction proceeds through S- and P-wave captures. The contributing RME in the limit of zero incident energy are listed in Table V. We note that M_2 transitions from the $L,S,J=1,3/2,5/2$ initial dp continuum state have been neglected. As in the dn capture, the effects due to two-body currents and Δ degrees of freedom are large on the M_1 RME, particularly the doublet M_1. The E_2 RME is very small, and the calculated value appears to be rather insensitive to the model Hamiltonian used.

Among the E_1 and M_2 RME from P-wave capture, the leading RME are the doublet $E_1^{1(1/2)J}$ with $J=1/2$, 3/2. The quartet $E_1^{1(3/2)J}$ ($M_2^{1(3/2)J}$) are about 1 order (2 orders) of magnitude smaller (in absolute value) than the $E_1^{1(1/2)J}$. While two-body current contributions for the doublet E_1 are small and have the same sign as the IA matrix element, they are found to be large, in fact dominant, for the quartet E_1, and of opposite sign than the IA contribution. Effects due to Δ isobar degrees of freedom are small, since the associated

TABLE VIII. Leading coefficients a_k, b_k, c_k, and d_k in nb in the Legendre expansions of $\sigma_u(\theta)$, $A_y(\theta)$, $T_{20}(\theta)$, and $P_\gamma(\theta)$, respectively, for the ^{2}H$(p,\gamma)^3$He capture reaction. The coefficients have been calculated with the AV18/IX Hamiltonian model at $E_p=10$, 25, 45 80, and 150 keV.

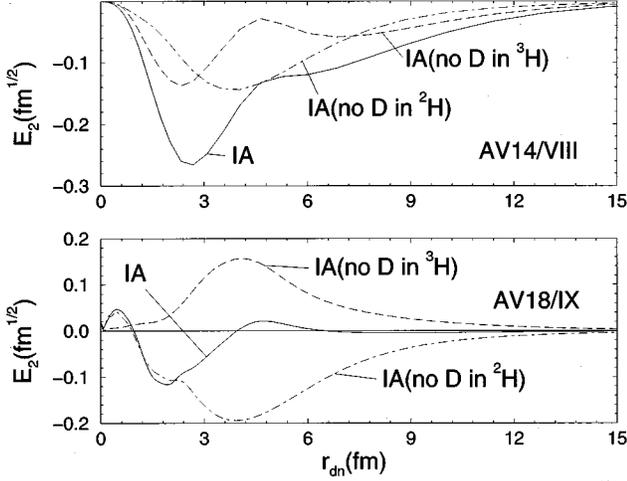| | | E_p | | | | |
		10	25	45	80	150
a_0	IA	0.0946	1.81	6.48	16.2	35.4
	IA+$\cdots$+Δ	0.130	2.44	8.49	20.7	45.2
a_2/a_0	IA	−0.619	−0.686	−0.769	−0.842	−0.900
	IA+$\cdots$+Δ	−0.536	−0.604	−0.694	−0.777	−0.850
b_1/a_0	IA	0.438	0.346	0.258	0.182	0.124
	IA+$\cdots$+Δ	0.145	0.114	0.0838	0.0575	0.0429
c_0/a_0	IA	0.0257	0.0266	0.0307	0.0328	0.0353
	IA+$\cdots$+Δ	−0.0814	−0.0908	−0.104	−0.117	−0.127
c_2/a_0	IA	0.242	0.192	0.131	0.0781	0.0297
	IA+$\cdots$+Δ	0.361	0.328	0.284	0.245	0.213
d_2/a_0	IA	0.309	0.343	0.384	0.421	0.450
	IA+$\cdots$+Δ	0.269	0.303	0.347	0.389	0.426

FIG. 5. The functions $\widetilde{E}_2^{0(3/2)(3/2)}(q;r_{dn})$ calculated with the AV14/VIII (top panel) and AV18/IX (bottom panel) Hamiltonian models in the IA (solid lines). The functions obtained by switching off either the deuteron (dot-dashed lines) or tritium (dashed lines) D states are also displayed.

FIG. 6. The functions $\widetilde{E}_1^{0(1/2)(1/2)}(q;r_{dp})$ and $\widetilde{E}_1^{0(3/2)(1/2)}(q;r_{dp})$ obtained with the AV18/IX Hamiltonian model in IA (empty symbols) and in the IA$+\cdots+\Delta$ approximation (solid symbols).

currents illustrated in Fig. 3 [with the exception of those arising from Figs. 3(f) and 3(h)–3(l)] are transverse.

We show in Fig. 6 the functions $\widetilde{E}_1^{1(1/2)(1/2)}(q;r_{dp})$ and $\widetilde{E}_1^{1(3/2)(1/2)}(q;r_{dp})$ (defined as in the previous subsection): the empty (solid) symbols correspond to the IA (IA $+\cdots+\Delta$) results. The doublet $J=1/2$ E_1 function is long-ranged, and is little affected by two-body current contributions. In contrast, the quartet $J=1/2$ E_1 function is fairly short-ranged, and changes sign when two-body currents are included. Similar features are exhibited by the doublet and quartet $J=3/2$ E_1 functions. The quartet E_1 RME are therefore sensitive to the short-range part of the nuclear wave functions, which is presumably the least accurately determined in the present variational calculations. Furthermore, as can be seen from Table V by comparing the IA+PS and IA+MI results for the quartet E_1 RME, the MI two-body currents of shorter range, particularly those associated with the momentum dependence of the NN interaction, give significant corrections. The precise form of these currents is rather uncertain [24].

To check the calculation of the E_1 RME, we have evaluated the appropriate combinations of $j_{\lambda\sigma_3}^{LSJJ_z}$ matrix elements making use of the identity valid in the long-wavelength (LW) approximation (which is justified in the energy range under consideration here)

$$j_{\lambda\sigma_3}^{LSJJ_z}(q;LW) = \langle \Psi_3^{(1/2)\sigma_3}| - \int d\mathbf{x}\epsilon^*(\mathbf{q})\cdot\mathbf{x}\nabla\cdot\mathbf{j}(\mathbf{x})|\overline{\Psi}_{2+1}^{LSJJ_z}\rangle$$

$$= i(E_f - E_i)\langle \Psi_3^{(1/2)\sigma_3}|$$

$$\times \int d\mathbf{x}\epsilon^*(\mathbf{q})\cdot\mathbf{x}\rho(\mathbf{x})|\overline{\Psi}_{2+1}^{LSJJ_z}\rangle, \qquad (6.9)$$

where $\mathbf{j}(\mathbf{x})$ and $\rho(\mathbf{x}) = \Sigma_i\delta(\mathbf{x}-\mathbf{r}_i')(1+\tau_{z,i})/2$ are the current and charge density operators, with $\mathbf{r}_i' = \mathbf{r}_i - \mathbf{R}_{c.m.}$, and E_i and E_f are the c.m. energies of the initial and final states. In
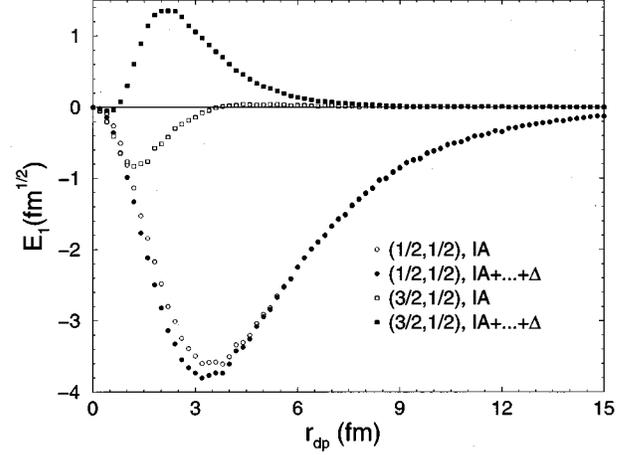
Table VI the results for the E_1 RME in the LW approximation are compared with those obtained by direct evaluation of Eq. (5.2). The two sets of results listed in Table VI correspond to the AV14 and AV14/VIII Hamiltonian models. The MI two-body currents, by construction, exactly satisfy current conservation with the AV14 interaction. Therefore, the degree of agreement between the LW and IA+MI AV14 results simply reflects the extent to which the present variational wave functions are truly exact eigenstates of the AV14 Hamiltonian. While the LW and IA+MI predictions for the doublet E_1 RME are quite close, those for the quartet E_1 RME are significantly different. Finally, as can be seen from Table VI by comparing the AV14 and AV14/VIII results, the effect of the three-nucleon interaction is not negligible. It is interesting to note that the continuity equation requires, in principle, the presence of three-body currents associated with it. The lack of these three-body currents is presumably partially responsible for the differences between the LW and IA+MI results, obtained with the AV14/VIII Hamiltonian.

We note that the numerically uncertain values of the E_1 RME impact our predictions for the S-factor and polarization observables at the 10% level. For example, at $E_{c.m.}=16$ keV and $\theta=30°$ the proton analyzing power is 0.095 or 0.086, depending on whether the IA$+\cdots+\Delta$ or LW values are used for these RME's.

The calculated S- and P-wave capture contributions to the zero-energy S factor are compared with the most recent experimental determinations [11] in Table VII. The $S_S(E_{c.m.}=0)$ is found to be 0.105 eV b, in good agreement with experiment, $S_S^{expt}(E_{c.m.}=0)=0.109\pm0.01$ eV b, and with the value reported in Ref. [18], 0.108 eV b. However, the experimental P-wave S factor, $S_P^{expt}(E_{c.m.}=0)=0.073\pm0.007$ eV b, is 15 (10) % smaller than calculated with the AV18/IX (AV14/VIII) Hamiltonian.

Results for the S factor in the energy range $E_p=0$–150 keV ($E_{c.m.}=0$–100 keV) are shown in Fig. 7, where they are compared with the recent TUNL data [11,13] and the much older data of Ref. [12]. Both the absolute values and energy dependence of the TUNL data are well reproduced by the IA
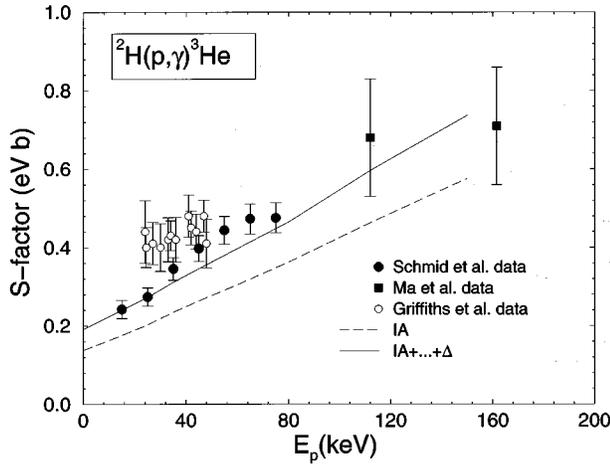
FIG. 7. The S factor of the ^{2}H(p,γ) ^{3}He reaction, obtained with the AV18/IX Hamiltonian model in the IA (long-dashed line) and in the IA$+\cdots+\Delta$ approximation (solid line) is compared with experimental results from Refs. [11–13].
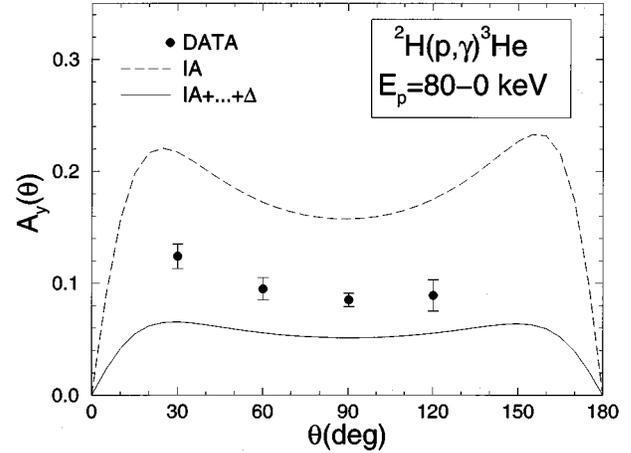

FIG. 9. The energy-integrated vector analyzing powers of the ^{2}H$(\vec{p},\gamma)$ ^{3}He reaction, obtained with the AV18/IX Hamiltonian model in the IA (dashed line) and in the IA$+\cdots+\Delta$ approximation (solid line), are compared with experimental results from Ref. [11].

$+\cdots+\Delta$ calculation. The enhancement due to two-body current and Δ-isobar contributions is substantial: the ratios $[S(\text{IA}+\cdots+\Delta)-S(\text{IA})]/S(\text{IA})$ for the S- and P-wave S factors are found to be, respectively, 0.62 and 0.18 at 0 keV, and increase to 0.75 and 0.22 at $E_p=150$ keV. The Griffith et al. data [12] have large errors, and appear to be at variance with the TUNL data.

The angular distributions of the energy-integrated relative cross section, vector and tensor analyzing powers, and photon linear polarization [11] are compared with theory in Figs. 8–11. As discussed in Ref. [11], the energy binning of the data would substantially increase the statistical errors. Accordingly, we have integrated the theoretical calculations, weighted by the energy dependence of the cross section and

the target thickness, for the purpose of comparing them with experiment [50]. However, it should be emphasized that the energy dependence of these observables is anyway rather weak.

The overall agreement between theory and experiment is satisfactory for all observables with the exception of $A_y(\theta)$. This latter observable is particularly sensitive to two-body current contributions: their effect is to reduce the results obtained in IA by about a factor of 3, bringing them into better agreement with the data. However, $a\simeq 30\%$ discrepancy between the predicted and measured A_y remains unresolved. It is important to recall here that these observables, unlike thermal cross sections, are independent of normalization issues in both theory and experiment.

The relative cross section and polarization observables appear to be rather insensitive to the Hamiltonian used. This
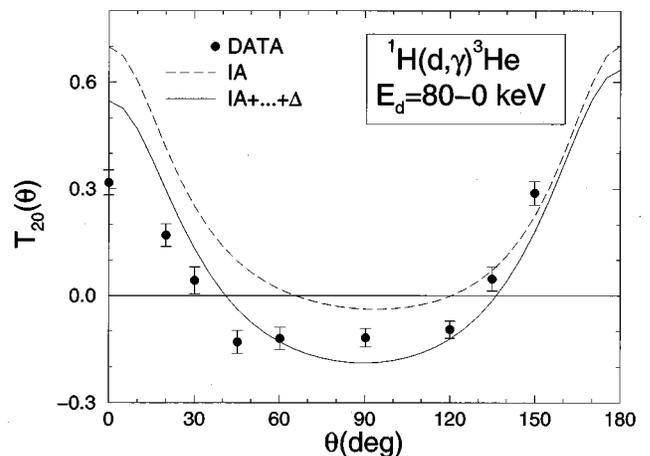

FIG. 8. The energy-integrated relative cross sections, $\sigma(\theta)/a_0$ ($4\pi a_0$ is the total cross section), obtained with the AV18/IX Hamiltonian model in the IA (dashed line) and in the IA$+\cdots+\Delta$ approximation (solid line), are compared with experimental results from Ref. [11]. Note that this plot only shows data with $E_p=0$–40 keV ($E_{c.m.}=0$–27 keV). This is done to allow the (d,γ) data with $E_d=0$–80 keV ($E_{c.m.}=0$–27 keV) and the (p,γ) data to be shown in the same graph [with the (d,γ) data reflected].

FIG. 10. The energy-integrated tensor analyzing powers of the ^{1}H$(\vec{d},\gamma)$ ^{3}He reaction, obtained with the AV18/IX Hamiltonian model in the IA (dashed line) and in the IA$+\cdots+\Delta$ approximation (solid line), are compared with experimental results from Ref. [11].
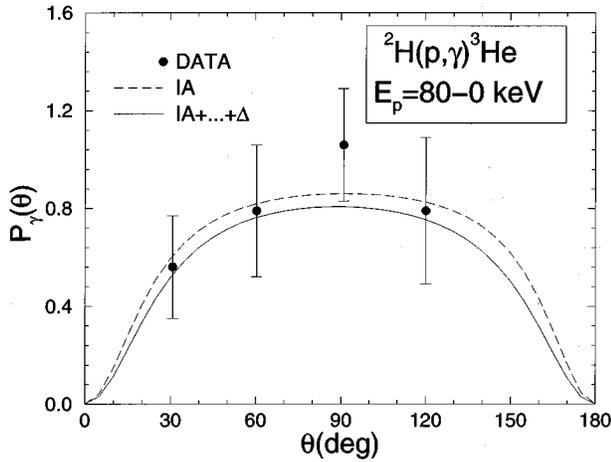
FIG. 11. Same as in Fig. 9, but for the photon linear polarization coefficient.

FIG. 13. Same as in Fig. 12, but for the tensor analyzing powers.

is shown in Figs. 12 and 13, where the vector and tensor analyzing powers calculated with the AV18/IX model are compared with those obtained from the AV14/VIII model. However, these observables, in particular the $A_y(\theta)$, are found to be sensitive to D-state components in either the initial or final states. This is shown in Figs. 14 and 15 for the $A_y(\theta)$ and $T_{20}(\theta)$ by switching off the D-state component in either the deuteron (dot-dashed line) or ^{3}He (dotted line) wave functions.

Finally, in Table VIII we list for completeness the values for the coefficients in the Legendre expansion of $\sigma_u(\theta)$, $A_y(\theta)$, $T_{20}(\theta)$, and $P_\gamma(\theta)$. We note that the total cross section is given by $4\pi a_0$.

VII. CONCLUSIONS

Cross sections and polarization observables for the ^{2}H$(\vec{p},\gamma)^3$He and ^{1}H$(\vec{d},\gamma)^3$He reactions below $E_{c.m.}=100$ keV, and for the thermal neutron radiative capture on deuterium have been calculated with accurate variational wave functions obtained from realistic interactions and an electro-

FIG. 12. The vector analyzing powers obtained with the AV14/VIII and AV18/IX Hamiltonian models in the IA and in the approximation IA$+\cdots+\Delta$ at $E_p=$ 25 keV.
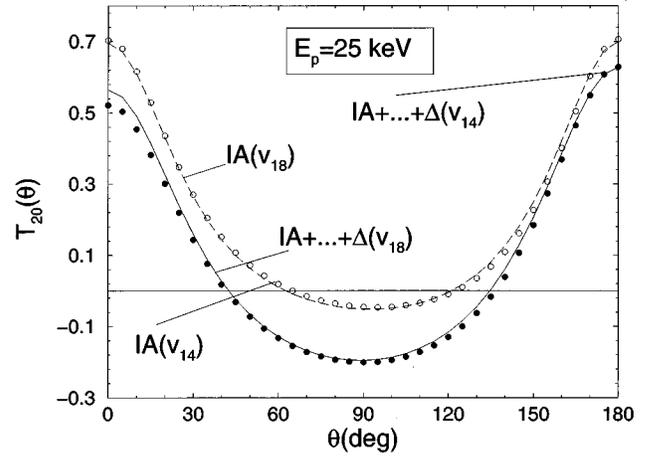
magnetic current operator consisting of one- and two-body parts. The wave functions include both nucleon and Δ-isobar degrees of freedom. The one-body currents contain $N\to N$, $N\to\Delta$, and $\Delta\to\Delta$ couplings, while only $NN\to NN$ terms have been retained in the two-body currents. The latter satisfy, by construction, current conservation exactly with the NN interaction.

Comparison between the theoretical results obtained with the more recent (and preferred) AV18/IX Hamiltonian model and data shows the following.

(1) The predicted values for the total cross section σ_T and photon polarization parameter R_c of the ^{2}H$(n,\gamma)^3$H reaction are within 15% of the measured values.

(2) The predicted energy dependence of the S factor and angular distributions of the cross section $\sigma_u(\theta)/\sigma_T$, tensor analyzing power $T_{20}(\theta)$, and photon linear polarization coefficient $P_\gamma(\theta)$ for the radiative capture of protons on deuterons in the center of mass energy range 0–100 keV are quite close to the experimental ones. However, the observed vector analyzing power $A_y(\theta)$ from ^{2}H$(\vec{p},\gamma)^3$He measurements is 30% larger than calculated.

The cross sections and polarization observables, in particular R_c and $A_y(\theta)$, are substantially affected by two-body currents, specifically the isovector ones associated with the tensor interaction. The R_c and $A_y(\theta)$ observables are also sensitive to D-state components in the deuteron and ^{3}He wave functions, and hence show an interesting interplay between two-body current effects and D-state admixtures in the ground state wave functions, both of which are induced by the tensor force.

The predictions based on the explicit inclusion of Δ-isobar degrees of freedom in the nuclear wave functions are found to be in significantly better agreement with experiment than those obtained from perturbation theory estimates.

To conclude, the overall, quantitative agreement between theory and experiment suggests that the nuclear dynamics at play in these complicated low-energy processes is fairly well understood. The remaining discrepancies between theory and experiment, such as the 30% underprediction of the measured vector analyzing power for the ^{2}H$(\vec{p},\gamma)^3$He reaction, indicate that further refinements are necessary in the present
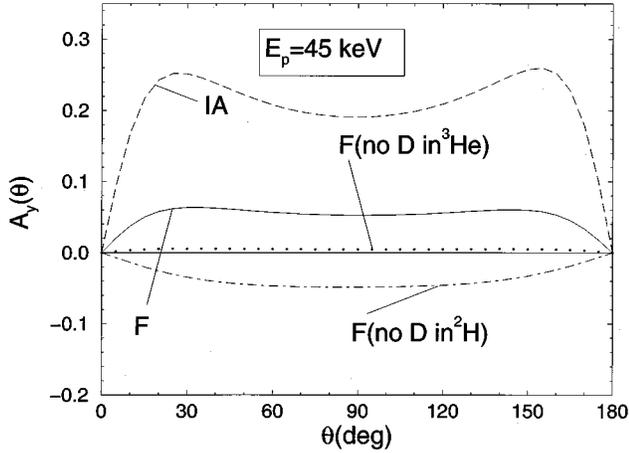
FIG. 14. The vector analyzing powers obtained with the AV14/VIII Hamiltonian model in the IA (dashed line) and in the approximation IA$+\cdots+\Delta$ (solid line labeled F) at $E_p=$ 45 keV. Also shown are the IA$+\cdots+\Delta$ results obtained by switching off the D-state components in either deuteron [dot-dashed line labeled F (no D in ^{2}H)] or ^{3}He [dotted line labeled F (no D in ^{3}He)].

FIG. 15. Same as in Fig. 14, but for the tensor analyzing powers.

theoretical framework. Examples of these are (1) the inclusion of three-body current contributions and (2) the inclusion of additional relativistic corrections of pionic range in the two-body current operators [55,56]. Work along these lines is being vigorously pursued. Furthermore, the measurement of other polarization observables, such as the T_{11} and T_{22} analyzing powers, which is currently under way at TUNL [13] will provide a new testing ground for theory.

Low-energy reactions remain an important area for studying nuclear dynamics, and a rich field for both theory and experiment.

ACKNOWLEDGMENTS

APPENDIX A: EXPRESSIONS FOR THE TWO-BODY CURRENT OPERATORS

In this appendix we provide complete expressions for the "model-independent" (MI) and "model-dependent" (MD) current operators. A thorough discussion of them can be found in Refs. [4,24,25].

The $\mathbf{j}^{(2)}_{ij,\mathrm{MI}}$ operators are constructed from the NN interaction. The Argonne v_{14} [28] and the charge-independent part of the new Argonne v_{18} [30] interaction models can be cast into the form

$$v_{ij}=\sum_{p=c,\sigma,t,so,so2,ll,ll\sigma}[v^p(r_{ij})+v^{p\tau}(r_{ij})\tau_i\cdot\tau_j]O^p_{ij}, \tag{A1}$$

$$O^{p=c,\ldots,ll\sigma}=1,\quad \sigma_i\cdot\sigma_j,S_{ij},\quad \mathbf{L}\cdot\mathbf{S},\quad \frac{1}{2}[\sigma_i\cdot\mathbf{L}\sigma_j\cdot\mathbf{L}+\mathrm{H.c.}],\quad \mathbf{L}^2,\mathbf{L}^2\sigma_i\cdot\sigma_j. \tag{A2}$$

Here S_{ij}, $\mathbf{L}$ and $\mathbf{S}$ are the tensor, orbital angular momentum and total spin operators of pair ij, respectively. Correspondingly we write

$$\mathbf{j}_{ij,\mathrm{MI}}=\sum_{p=PS,V,SO,SO2,LL}\mathbf{j}_{ij,p}, \tag{A3}$$

where $\mathbf{j}_{ij,PS}$ and $\mathbf{j}_{ij,V}$ have already been given in Eqs. (3.8) and (3.9), and

$$\mathbf{j}_{ij,SO}(\mathbf{k}_i,\mathbf{k}_j)=-\frac{i}{8m^2}[P(j)[v^c(k_i)+2m^2v^{so}(k_i)][(\sigma_i+\sigma_j)\times\mathbf{k}_i-i(\mathbf{p}_i+\mathbf{p}'_i)]+Q(i)[v^{c\tau}(k_i)+2m^2v^{so\tau}(k_i)]$$

$$\times[(\sigma_i+\sigma_j)\times\mathbf{k}_i-i(\mathbf{p}_i+\mathbf{p}'_i)]+P(j)[3v^c(k_i)-2m^2v^{so}(k_i)][\sigma_j\times\mathbf{q}-i(\mathbf{p}_j+\mathbf{p}'_j)]+i\rightleftharpoons j], \tag{A4}$$

$$\mathbf{j}_{ij,SO2}(\mathbf{q}) = \frac{1}{8}[v^{so2}(r_{ij})D_+(\mathbf{q}) + v^{so2\tau}(r_{ij})D'_+(\mathbf{q})]\boldsymbol{\sigma}_i \cdot (\mathbf{r}_{ij} \times \mathbf{q})\boldsymbol{\sigma}_j \times \mathbf{r}_{ij}$$

$$+ \frac{1}{4}[v^{so2}(r_{ij})D_-(\mathbf{q}) + v^{so2\tau}(r_{ij})D'_-(\mathbf{q})]\{\boldsymbol{\sigma}_i \cdot \mathbf{L}, \boldsymbol{\sigma}_j \times \mathbf{r}_{ij}\} + i \rightleftharpoons j, \tag{A5}$$

$$\mathbf{j}_{ij,LL}(\mathbf{q}) = [v^{ll}(r_{ij}) + v^{ll\sigma}(r_{ij})\boldsymbol{\sigma}_i \cdot \boldsymbol{\sigma}_j][D_-(\mathbf{q})(i|P)\mathbf{r}_{ij} - \mathbf{r}_{ij} \times \mathbf{L}) - \frac{1}{4}D_+(\mathbf{q})\mathbf{r}_{ij} \times (\mathbf{r}_{ij} \times \mathbf{q})] + [v^{ll\tau}(r_{ij}) + v^{ll\sigma\tau}(r_{ij})\boldsymbol{\sigma}_i \cdot \boldsymbol{\sigma}_j]$$

$$\times \left[D'_-(\mathbf{q})(i\mathbf{r}_{ij} - \mathbf{r}_{ij} \times \mathbf{L}) - \frac{1}{4}D'_+(\mathbf{q})\mathbf{r}_{ij} \times (\mathbf{r}_{ij} \times \mathbf{q}) \right], \tag{A6}$$

where $\mathbf{p}_i$ and $\mathbf{p}'_i$ are the initial and final momentum of nucleon i. We have also defined

$$P(i) \equiv \frac{1 + \tau_{z,i}}{2}, \tag{A7}$$

$$Q(i) \equiv \frac{\boldsymbol{\tau}_i \cdot \boldsymbol{\tau}_j + \tau_{z,i}}{2}, \tag{A8}$$

$$D_\pm(\mathbf{q}) \equiv P(i)e^{i\mathbf{q}\cdot\mathbf{r}_i} \pm P(j)e^{i\mathbf{q}\cdot\mathbf{r}_j}, \tag{A9}$$

$$D'_\pm(\mathbf{q}) \equiv Q(j)e^{i\mathbf{q}\cdot\mathbf{r}_i} \pm Q(i)e^{i\mathbf{q}\cdot\mathbf{r}_j}. \tag{A10}$$

The momentum-space components of the interaction, in terms of which are defined the current operators in Eqs. (3.8), (3.9), and (A.4), are given by

$$v^{\sigma\tau}(k) = \frac{4\pi}{k^2} \int_0^\infty dr r^2 [j_0(kr) - 1] v^{\sigma\tau}(r), \tag{A11}$$

$$v^{t\tau}(k) = \frac{4\pi}{k^2} \int_0^\infty dr r^2 j_2(kr) v^{t\tau}(r), \tag{A12}$$

$$v^p(k) = 4\pi \int_0^\infty dr r^2 j_0(kr) v^p(r), \quad p = c, c\tau, \tag{A13}$$

$$v^p(k) = -\frac{4\pi}{k} \int_0^\infty dr r^3 j_1(kr) v^p(r), \quad p = so, so\tau. \tag{A14}$$

The MD two-body current operator consists of the terms associated with the $\rho\pi\gamma$ and $\omega\pi\gamma$ contributions:

$$\mathbf{j}^{(2)}_{ij,\text{MD}}(\mathbf{k}_i, \mathbf{k}_j) = \mathbf{j}_{ij,\rho\pi\gamma}(\mathbf{k}_i, \mathbf{k}_j) + \mathbf{j}_{ij,\omega\pi\gamma}(\mathbf{k}_i, \mathbf{k}_j) \tag{A15}$$

with

$$\mathbf{j}_{\rho\pi\gamma}(\mathbf{k}_i, \mathbf{k}_j) = i\frac{f_\pi g_\rho g_{\rho\pi\gamma}}{m_\pi m_\rho} \boldsymbol{\tau}_i \cdot \boldsymbol{\tau}_j \mathbf{k}_i \times \mathbf{k}_j \left[\frac{\boldsymbol{\sigma}_i \cdot \mathbf{k}_i}{(k_i^2 + m_\pi^2)(k_j^2 + m_\rho^2)} - \frac{\boldsymbol{\sigma}_j \cdot \mathbf{k}_j}{(k_i^2 + m_\rho^2)(k_j^2 + m_\pi^2)} \right], \tag{A16}$$

$$\mathbf{j}_{\omega\pi\gamma}(\mathbf{k}_i, \mathbf{k}_j) = i\frac{f_\pi g_\omega g_{\omega\pi\gamma}}{m_\omega m_\pi} \mathbf{k}_i \times \mathbf{k}_j \left[\frac{\boldsymbol{\sigma}_i \cdot \mathbf{k}_i}{(k_i^2 + m_\pi^2)(k_j^2 + m_\omega^2)} \tau_{i,z} - \frac{\boldsymbol{\sigma}_j \cdot \mathbf{k}_j}{(k_i^2 + m_\omega^2)(k_j^2 + m_\pi^2)} \tau_{j,z} \right]. \tag{A17}$$

For the $\rho\pi\gamma$, $\omega\pi\gamma$, and ωNN coupling constants we use the values 0.56 and 0.63 (from the measured widths of $\rho \to \pi + \gamma$ [51] and $\omega \to \pi + \gamma$ [52]) and 14.6 (from the Bonn potential [53]), respectively. We introduce monopole form factors at the pion and vector meson vertices in the $\rho\pi\gamma$ and $\omega\pi\gamma$ two-body current operators with $\Lambda_\pi = 0.75$ GeV, and $\Lambda_\rho = \Lambda_\omega = 1.25$ GeV. The values used for Λ_π and Λ_ρ have been taken from a study of the $\rho\pi\gamma$ current contribution to the $B(q)$ structure function of the deuteron [54].

Finally, the configuration-space expressions for the current operators in Eqs. (3.8), (3.9), and (A.4) are obtained from [24]

$$\mathbf{j}_{ij,a}(\mathbf{q}) = \int d\mathbf{x} e^{i\mathbf{q}\cdot\mathbf{x}} \int \frac{d\mathbf{k}_i}{(2\pi)^3} \frac{d\mathbf{k}_j}{(2\pi)^3} e^{i\mathbf{k}_i \cdot (\mathbf{r}_i - \mathbf{x})} e^{i\mathbf{k}_j \cdot (\mathbf{r}_j - \mathbf{x})} \mathbf{j}_{ij,a}(\mathbf{k}_i, \mathbf{k}_j). \tag{A18}$$

APPENDIX B: EXPRESSIONS FOR R_c AND FOR THE LEADING COEFFICIENTS IN THE LEGENDRE EXPANSIONS OF THE OBSERVABLES

In this appendix we list the expressions for the photon polarization parameter R_c and for leading coefficients a_k, b_k, c_k, and d_k in the Legendre expansions Eqs. (4.20)–(4.23) of the cross section and polarization observables. In the energy range of interest in the present study, the leading contributions are those associated with electric and magnetic dipole transitions, while the contributions due to higher order multipoles, although included in the results reported in Sec. VI, are found to be numerically very small and, therefore, are not explicitly displayed in the formulas below for ease of presentation (with the exception of R_c). We also use the notation

$$m_{2S+1\ 2J+1} = \widetilde{M}_1^{0SJ}, \tag{B1}$$

$$p_{2S+1\ 2J+1} = \widetilde{E}_1^{1SJ}, \tag{B2}$$

and

$$\sigma_1 = \frac{1}{4\pi} \frac{2}{9} \frac{\alpha}{v_{\text{rel}}} \frac{q^3}{4m^2}. \tag{B3}$$

The leading coefficients in the expansion for $\sigma_u(\theta)$ are a_0 and a_2, and their expressions are

$$a_0 = \sigma_1[|m_{22}|^2 + |m_{44}|^2 + |p_{22}|^2 + |p_{42}|^2 + |p_{24}|^2 + |p_{44}|^2], \tag{B4}$$

$$a_2 = \frac{1}{10}\sigma_1[10\sqrt{2}\text{Re}(p_{22}p_{24}^*) - 2\sqrt{5}\text{Re}(p_{42}p_{44}^*) - 5|p_{24}|^2 + 4|p_{44}|^2]. \tag{B5}$$

In the expansion for the vector analyzing power A_y the leading coefficient is b_1, and its expression is

$$b_1 = \frac{\sqrt{2}}{6}\sigma_1\text{Re}[m_{22}^*(-\sqrt{8}p_{22} + 4p_{42} + p_{24} + \sqrt{20}p_{44})] + \frac{1}{6}\sigma_1\text{Re}[m_{44}^*(-\sqrt{8}p_{22} - 5p_{42} + 10p_{24} + \sqrt{20}p_{44})]. \tag{B6}$$

In the expansion for the tensor analyzing power T_{20} the leading coefficients are c_0 and c_2, and their expressions are

$$c_0 = \sqrt{\frac{2}{6}}\sigma_1\text{Re}[10\sqrt{2}\text{Re}(p_{22}p_{42}^*) - 5|p_{42}|^2 - 2\sqrt{5}\text{Re}(p_{24}p_{44}^*) + 4|p_{44}|^2], \tag{B7}$$

$$c_2 = \sigma_1\left[-\text{Re}(m_{22}m_{44}^*) + \sqrt{\frac{1}{8}}|m_{44}|^2 - \sqrt{\frac{1}{5}}\text{Re}(p_{22}p_{44}^*) + \sqrt{2}\ \text{Re}(p_{42}p_{24}^*) + \sqrt{\frac{1}{10}}\text{Re}(p_{42}p_{44}^*) + \sqrt{\frac{1}{10}}\text{Re}(p_{24}p_{44}^*) + \sqrt{\frac{1}{8}}|p_{44}|^2\right]. \tag{B8}$$

In the expansion for the photon linear coefficient P_γ the leading coefficient is d_2, and its expression is

$$d_2 = \sigma_1\left[-\sqrt{\frac{1}{2}}\text{Re}(p_{22}p_{24}^*) + \sqrt{\frac{1}{20}}\text{Re}(p_{42}p_{44}^*) + \frac{1}{4}|p_{24}|^2 - \frac{1}{5}|p_{44}|^2\right]. \tag{B9}$$

The photon polarization parameter R_c for S-wave capture is given by

$$R_c = -\frac{1}{3}\left[1 - \frac{(7/2)|m_{44}|^2 + \sqrt{8}\text{Re}(m_{22}m_{44}^*) + (5/2)|e_{44}|^2 + \sqrt{24}\text{Im}(m_{22}e_{44}^*) - \sqrt{3}\text{Im}(m_{44}e_{44}^*)}{|m_{22}|^2 + |m_{44}|^2 + |e_{44}|^2}\right]. \tag{B10}$$

Here the contribution of the electric quadrupole $e_{44} = \widetilde{E}_2^{0(3/2)(3/2)}$ is explicitly included. Finally, we note a misprint in Ref. [3], the interference term $\text{Re}(m_{22}m_{44}^*)$ between the doublet and quartet M_1 transitions in R_c is erroneously multiplied by a factor $\sqrt{2}$ rather than $\sqrt{8}$.

[1] C.E. Rolfs and W.S. Rodney, *Cauldrons in the Cosmos* (University of Chicago Press, Chicago, 1988).

[2] E.W. Kolb and M.S. Turner, *The Early Universe* (Addison-Wesley Publishing Company, Reading, MA, 1990).

[3] J.L. Friar, B.F. Gibson, and G.L. Payne, Phys. Lett. B **251**, 11 (1990).

[4] J. Carlson *et al.*, Phys. Rev. C **42**, 830 (1990).

[5] E.T. Jurney, P.J. Bendt, and J.C. Browne, Phys. Rev. C **25**, 2810 (1982).

[6] L. Kaplan, G.R. Ringo, and K.E. Wilzbach, Phys. Rev. **87**, 785 (1952).

[7] J.S. Merritt, J.G.V. Taylor, and A.W. Boyd, Nucl. Sci. Eng. **34**, 195 (1968).

[8] M.W. Konijnenberg *et al.*, Phys. Lett. B **205**, 215 (1988).

[9] M.W. Konijnenberg, Ph.D thesis, Netherlands Energy Research Foundation, 1990.

[10] G.J. Schmid *et al.*, Phys. Rev. C **52**, 1732 (1995).

[11] G.J. Schmid *et al.*, Phys. Rev. Lett. **76**, 3088 (1996).

[12] G.M. Griffiths, M. Lal, and C.D. Scarfe, Can. J. Phys. **41**, 724 (1963).

[13] L. Ma, C. Brune, H. Karwowski, and E. Ludwig, private communication.

[14] L.I. Schiff, Phys. Rev. **52**, 242 (1937).

[15] A.C. Phillips, Nucl. Phys. **A184**, 337 (1972).

[16] E. Hadjimichael, Phys. Rev. Lett. **31**, 183 (1973).

[17] J. Torre and B. Goulard, Phys. Rev. C **28**, 529 (1983).

[18] J.L. Friar *et al.*, Phys. Rev. Lett. **66**, 1827 (1991).

[19] A. Kievsky, S. Rosati, and M. Viviani, Nucl. Phys. **A551**, 241 (1993).

[20] A. Kievsky, S. Rosati, and M. Viviani, Nucl. Phys. **A577**, 511 (1994).

[21] A. Kievsky, M. Viviani, and S. Rosati, Phys. Rev. C **52**, R15 (1995).

[22] D. Hüber *et al.*, Phys. Rev. C **51**, 1100 (1995)

[23] R. Schiavilla *et al.*, Phys. Rev. C **45**, 2628 (1992).

[24] R. Schiavilla, V.R. Pandharipande, and D.O. Riska, Phys. Rev. C **40**, 2294 (1989).

[25] R. Schiavilla and D.O. Riska, Phys. Rev. C **43**, 437 (1991).

[26] M. Fabre de la Ripelle, Ann. Phys. (N.Y.) **147**, 281 (1983).

[27] G. Erens, J.L. Visschers, and R. van Wageningen, Ann. Phys. (N.Y.) **147**, 281 (1971).

[28] R.B. Wiringa, R.A. Smith, and T.L. Ainsworth, Phys. Rev. C **29**, 1207 (1984).

[29] R.B. Wiringa, Phys. Rev. C **43**, 1585 (1991).

[30] R.B. Wiringa, V.G.J. Stoks, and R. Schiavilla, Phys. Rev. C **51**, 38 (1995).

[31] B.S. Pudliner *et al.*, Phys. Rev. Lett. **74**, 4396 (1995).

[32] W. Glöckle *et al.*, Few Body Syst. Suppl. **8**, 9 (1995)

[33] C.R. Chen *et al.*, Phys. Rev. C **31**, 2266 (1985).

[34] C.R. Chen *et al.*, Phys. Rev. C **44**, 50 (1991).

[35] W. Dilg, L. Koester, and W. Nistler, Phys. Lett. **36B**, 208 (1971).

[36] C.R. Chen *et al.*, Phys. Rev. C **33**, 1740 (1986).

[37] J. Carlson, Nucl. Phys. **A508**, 141c (1990).

[38] A.C. Phillips, Phys. Rev. **142**, 984 (1966).

[39] C.E. Carlson, Phys. Rev. D **34**, 2704 (1986).

[40] D. Lin and M.K. Liou, Phys. Rev. C **43**, R930 (1991).

[41] T.E.O. Ericson and W. Weise, *Pions and Nuclei* (Clarendon Press, Oxford, 1988).

[42] D.O. Riska, Phys. Scr. **31**, 471 (1985).

[43] D.O. Riska, Prog. Part. Nucl. Phys. **11**, 199 (1984).

[44] T. deForest and J.D. Walecka, Adv. Phys. **15**, 1 (1966).

[45] A. Messiah, *Quantum Mechanics* (North-Holland Publishing Company, Amsterdam, 1961).

[46] R.G. Seyler and H.R. Weller, Phys. Rev. C **20**, 453 (1979).

[47] J. Lomnitz-Adler, V.R. Pandharipande, and R.A. Smith, Nucl. Phys. **A361**, 399 (1981).

[48] N. Metropolis *et al.*, J. Chem. Phys. **21**, 1087 (1953).

[49] A. Arriaga, V.R. Pandharipande, and R. Schiavilla, Phys. Rev. C **43**, 983 (1991).

[50] B.J. Rice, G.J. Schmid, and H.R. Weller, private communication.

[51] D. Berg *et al.*, Phys. Rev. Lett. **44**, 706 (1980).

[52] M. Chemtob and M. Rho, Nucl. Phys. **A163**, 1 (1971).

[53] K. Holinde and R. Machleidt, Nucl. Phys. **A256**, 479 (1976).

[54] J. Carlson, V.R. Pandharipande, and R. Schiavilla, in *Modern Topics in Electron Scattering*, edited by B. Frois and I. Sick (World Scientific, Singapore, 1991), p. 177.

[55] J.L. Friar, Ann. Phys. (N.Y.) **104**, 380 (1976).

[56] J.L. Friar, Phys. Lett. **69B**, 51 (1977).